Mechanical and electrical properties of 3D-printed acrylonitrile butadiene styrene composites reinforced with carbon nanomaterials

by

Abigail Weaver

B.S., Kansas State University, 2014

_____

A THESIS

submitted in partial fulfillment of the
requirements for the degree

MASTER OF SCIENCE

Department of Mechanical and Nuclear Engineering
College of Engineering

KANSAS STATE UNIVERSITY
Manhattan, Kansas

2017

Approved by:

Major Professor
Gurpreet Singh

Copyright

Abstract

3D-printing is a popular manufacturing technique for making complex parts or small quantity batches. Currently, the applications of 3D-printing are limited by the material properties of the printed material. The processing parameters of commonly available 3D-printing processes constrain the materials used to a small set of primarily plastic materials, which have relatively low strength and electrical conductivity. Adding filler materials has the potential to improve these properties and expand the applications of 3D printed material. Carbon nanomaterials show promise as filler materials due to their extremely high conductivity, strength, and surface area.

In this work, Graphite, Carbon Nanotubes, and Carbon Black (CB) were mixed with raw Acrylonitrile Butadiene Styrene (ABS) pellets. The resulting mixture was extruded to form a composite filament. Tensile test specimens and electrical conductivity specimens were manufactured by Fused Deposition Method (FDM) 3D-printing using this composite filament as the feedstock material. Weight percentages of filler materials were varied from 0-20 wt% to see the effect of increasing filler loading on the composite materials. Additional tensile test specimens were fabricated and post-processed with heat and microwave irradiation in attempt to improve adhesion between layers of the 3D-printed materials.

Electrical Impedance Spectroscopy tests on 15 wt% Multiwalled Carbon Nanotube (MWCNT) composite specimens showed an increase in DC electrical conductivity of over 6 orders of magnitude compared to neat ABS samples. This 15 wt% specimen had DC electrical conductivity of $8.74x10^-6$ S/cm, indicating semi-conducting behavior. MWCNT specimens with under 5 wt% filler loading and Graphite specimens with under 1 wt% filler loading showed strong insulating behavior similar to neat ABS.

Tensile tests showed increases in tensile strength at 5 wt% CB and 0.5 wt% MWCNT. Placing the specimens in the oven at 135 °C for an hour caused increased the stiffness of the composite specimens.

Table of Contents

List of Figures

List of Tables

Acknowledgments

First, I would like to thank my major professor, Dr. Singh, for his support, encouragement, and expert advice throughout the course of this project. My committee members Dr. Lease and Dr. Betz also provided valuable input. I especially appreciate Dr. Betz allowing me to use her lab groups optical microscope. Graduate students Michael Heidlage, Pedram Parandoush, and Kasun Fernando Thank you for training me to use your equipment. My assistants Diana Arreola and Gabrielle Biby helped me manufacture the many test specimens used in this project, and I am very glad to have had their assistance. I am grateful Dr. Meng Zhang and Dr. Dong Lin and their lab groups for their cooperation and for making their equipment available to me. I would also like to think Dr. Elisabeth Mansfield at NIST for running the TGA test from the samples I provided. Finally, my parents and family showed me incredible love and kindness throughout this project, and I am very grateful for their support.

Chapter 1

Introduction

1.1 Background and Motivation

Since its invention in the 1980s, Three-dimensional (3D) printing has gained tremendous popularity as a manufacturing process. Various type of 3D printing have been developed. All involve computer controlled, layer-by-layer deposition of materials in precise geometries. This process allows creation of complex geometries not possible by other manufacturing methods. Unlike casting processes, a variety of complex shapes can be created with no additional hardware. This makes 3D printing ideal for small quantity batches of complex parts. Each 3D printing process has restrictions on the type of material it can produce. Standard Fused Deposition Method can only print thermoplastic materials. The applications of FDM printed parts are limited by the material properties of these plastics which have low strength and are strong insulators. This restricts the printed parts to use to low stress applications. Academic researchers and industry professionals have been able to improve FDM material properties by adding filler materials to the base thermoplastics. The resulting composite material has is a hybrid of the two materials. Among potential filler materials, micro- and nanoscale fillers can be easily added without modifying the printing apparatus as is necessary for continuous fiber composites. Nanoscale fillers have the advantage of higher surface area and aspect compared to their micro-scale counterparts. Carbon fillers have the advantage of high tensile strength

and conductivity, making them a good choice for use as a filler material.

1.2 Goals and Strategy

The overall goal of this research was to improve the material and electrical properties of 3D printed materials in order to expand the applications of this novel manufacturing technique. Carbon fillers have high mechanical strength and conductivity. Including them as a filler material in existing 3D printing material has strong potential to create a strong, electrically conductive material that can be processed with existing machinery. As FDM is a very accessible 3D printing technology, and ABS is a common material used in FDM, FDM printed ABS plastic was chosen as the base material for this experiment. The specific goal of this research was to determine how the tensile properties and electrical conductivity changed with increasing weight percentages of carbon fillers. Graphite, Carbon Black, Multi-Walled Carbon Nanotubes and Single-Walled Carbon Nanotubes were used to create test specimens with varying weight concentrations. This thesis is organized six chapters, including the introduction. The remaining chapters cover the following topics: Chapter 2 contains background information about 3D printing and nanocomposites and a literature review of previous work in ABS nanocomposites. Chapter 3 describes the materials used and the experimental process for each test performed. Chapter 4 explains the material characterization tests used in this thesis and presents the data and conclusions provided by them. Chapter 5 presents results of tensile and conductivity tests and images of the fracture surfaces. It also discusses probable causes of the results found. Chapter 6 details the conclusions of this research and provides recommendations for continued research in 3D printed composites.

Chapter 2

Literature Review

This chapter provides an overview of existing knowledge relevant to the experimental work done in later chapters. In this chapter, I will discuss the significance of additive manufacturing, its applications and limitations, as welll as the difference between prominent types of additive manufacturing. Because improved material properties are one of the major growth areas for additive manufacturing, I will explain the potential for composite materials to overcome these difficulties. Then I will present information about various common nanomaterials that are well suited for use in composite materials and discuss the results of previous work on FDM-printed composite materials.

2.1   3D Printing and Additive Manufacturing

Additive manufacturing is a term that refers to a group of relatively new manufacturing techniques that form a desired shape by fusing pieces of raw material together. Generally the parts are in a series of layers that stack to make the final shape. Additive manufacturing can also be referred to as 3D printing, as there is no difference between the two terms. In contrast to additive manufacturing, many other manufacturing methods are a form of subtractive manufacturing. Rather than building up pieces of material, these processes start with a block, plate, or sheet of bulk material. Then surplus material is removed to make the
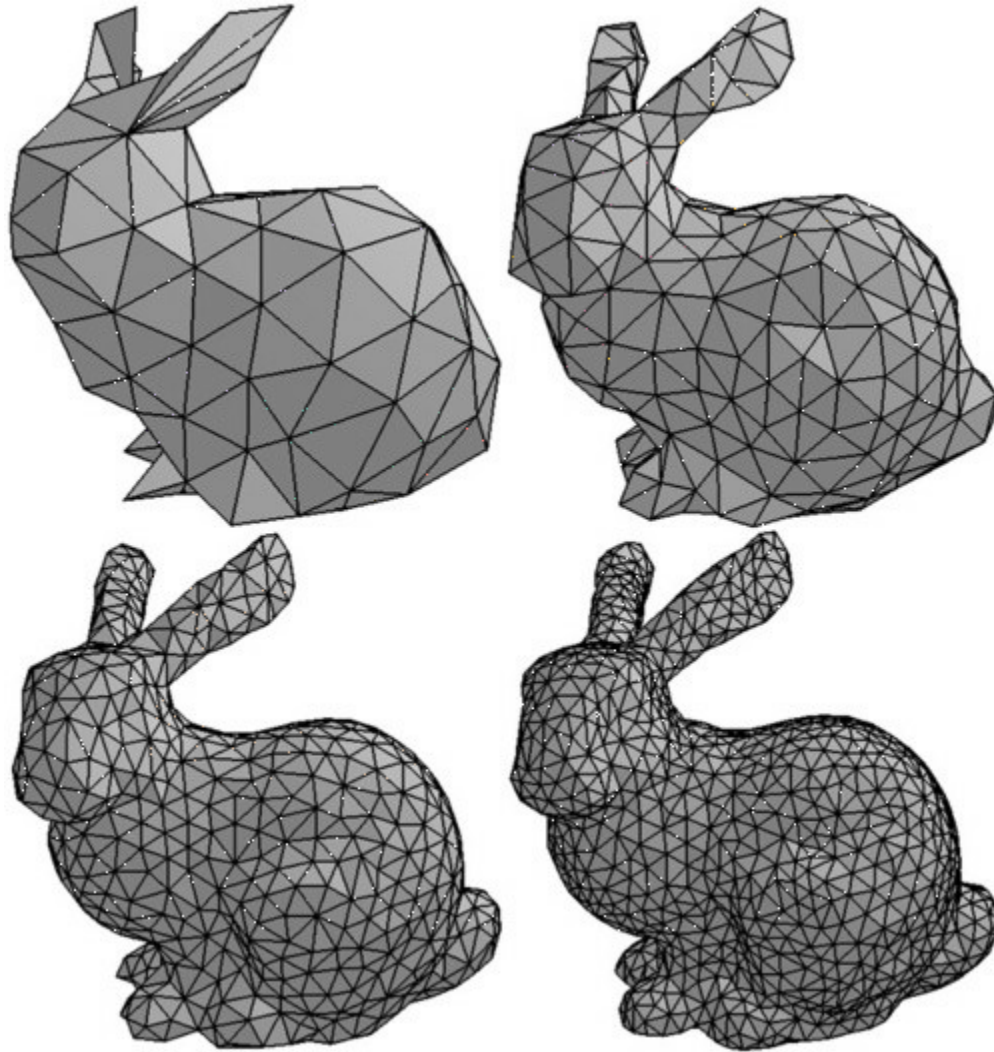
Figure 2.1: Bunny in stl file format with different resolutions. Copied from [1]

required shape. This extra material becomes a powder or a piece of scrap material which cannot be used again, but must be recycled or thrown away.

Additive manufacturing was started in the 1980's when the first 3D printers were manufactured, and over time many different methods of additive manufacturing were developed. These different processes, although they differ significantly and have varying strengths and applications, all share common characteristics. Common to all methods of 3D printing, is a dedicated machine designed for 3D printing and software that converts a 3D computer model of the part into a series of instructions for the machine. The process of creating a new part using a 3D printer first involves modeling the desired geometry in a 3D modeling

software or computer assisted design (CAD) program. Once the part geometry has been created digitally, the part is saved as a stereolithography file (.stl), a specific file format used by 3D printer software. Named after an early type of additive manufacturing, the .stl file encodes a set of triangles that mimic the shape of the 3D part. As shown in Fig. 2.1, the resolution, or number of triangles used per unit area, must be high enough to capture the geometry of the part correctly. Once the .stl file is imported into the 3D printer software, the user sets relevant printing parameters and chooses in what orientation to print the part. Then the software slices the part into layers, and translates the part geometry and print parameters into g-code, a type of machine code. The g-code is input to the 3D printer, giving the machine the precise step-by-step instructions necessary to create the desired part.

2.1.1   3D Printing: Strengths and Challenges

The strengths of 3D printing center on its ability to create a wide variety of complex shapes and parts with a single machine. A 3D printer can print a part with elaborate geometry without the need for new tooling or a complex setup of the machine. This means one-off or customizable parts are easy to make on a 3D printer, although they would very costly and slow to make through casting or machining. Parts can be produced rapidly because no new tooling is required, and the same machine can be used for multiple disparate projects. Small batches of parts are more economically feasible than they would be through other methods. Additionally, additive manufacturing can produce very complex shapes that cannot be manufactured by any other method. Furthermore, shipping times and costs for parts can be reduced by making them on-site rather than at a factory or supplier. Because of the strengths of additive manufacturing it is one of the preferred methods of rapid prototyping.

However, additive manufacturing has faults that make it not the best choice for every application. The limited material choices available for additive manufacturing may not have the correct properties (e.g. strength, conductivity) for an application. The size of a 3D printed part is limited by the dimensions of the printing area of the printer The resulting parts will likely be anisotropic, which may not be desirable. Most 3D printed objects have

(a)

(b)

(c)
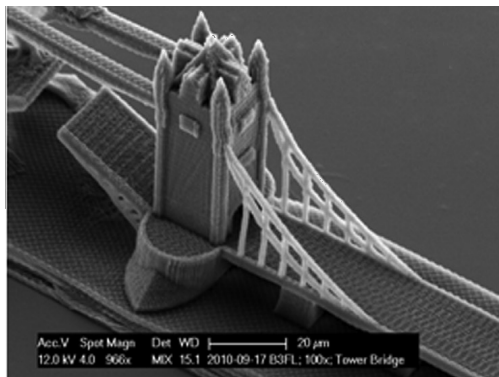
(d)

Figure 2.2: Additive manufacturing capabilities: (a) The text on this 3D printed phone case could be easily customized (b) This balls in this bearing were printed in place as the entire part was made (c) A metal replica of a jet engine manufactured by Selective Laser Sintering (d) a tiny model of a bridge made from a photosensitive polymer and manufactured with additive manufacturing technology. Adapted from [2–5]

a visible layered pattern visible on the part surface. Painting or other post-processing may be required before use. When production quantities are scaled up, additive manufacturing is not as competitive. While a specialized manufacturing process can produce hundreds of parts per hour, each 3D printer could take 20 min to a day per part depending on its size and complexity. Although the printing parameters can be adjusted to speed up the manufacturing process somewhat, print resolution and part quality will decline. So when large quantities of parts are required, other methods are generally more economical.

2.1.2 Types of Additive Manufacturing and Their Characteristics

Although there are many variations on additive manufacturing, the most prominent technologies are are stereolithography (STL), Fused deposition modeling (FDM), Selective Laser Sintering (SLS), and 3D Printing(3DP). Stereolithography is the oldest type of additive manufacturing[6;19] and was first developed by 3D Systems, Inc.[6]. Figure 2.3 shows a simplified schematic of the process. It involves liquid photosensitive resin that cures into a solid polymer when exposed to ultraviolet (UV) light. UV light causes monomers and polymers in the resin to polymerize into a solidified polymer. A base is submerged in a vat of photopolymer. The part is built onto the base as it is cured one layer at a time. Usually, a UV laser is used to provide a precise source of UV light. Each layer has whatever two-dimensional shape required at that level in order to form the final part. In between curing each layer the base and part are moved together one layer height. Then the next layer is ready to be cured with UV light. It is difficult to change materials mid-part as the polymer compound must be drained out and the vat cleaned in between each material. Certain shapes are not desirable because they cause sections of the photopolymer to be exposed to UV light repeatedly - leading to overexposure of part of the plastic. The shape is also limited by needing to be connected to the base at all times. Support structures may be needed for certain geometries or orientations. These supports must be removed later.

In SLS, a laser fuses powder together to form the desired geometry. A piston base is submerged in a bed of powder which is heated near the melting temperature of the powdered

7
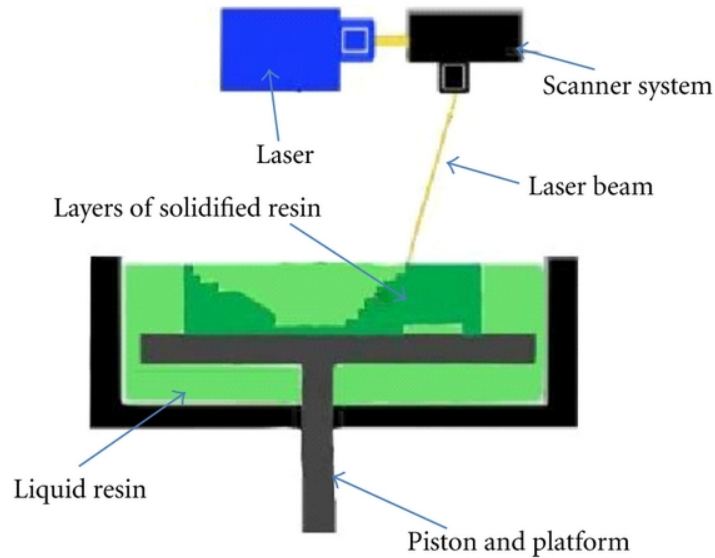
Figure 2.3: Simplified schematic of Stereolithography process. Figure copied from [6]

material. Before each layer rollers smooth powder over the top of the piston to form a smooth surface. The laser traces the desired path and melts the powder, binding it together and to the layer below it. Then the piston lowers deeper into the bed carrying the part with it. Rollers sweep more powder over the top and the process repeats until the part is completed. After printing, excess powder is cleaned from the crevices of the part and recycled. This method shares the difficulty of material changing with the STL process. However, over-curing is not a concern in SLS. SLS has a wide range of possible materials such as, plastics, metals, metal-polymer mixtures, and metal-ceramic mixtures. Metals require binder with a lower melting temperature such as a polymer or another metal in order to be processed. An inert atmosphere is needed to avoid oxidation during the process. The accuracy and tolerances of the part are limited by the size of particles in the powder. Another additive manufacturing technique based on SLS, Electron Beam Melting (EBM), expands the technology by using an high voltage (30-60 KV[6]) electron laser beam to melt the particles together. EBM is most often used to manufacture metal parts. Because of this it contains a vacuum chamber to prevent oxidation of the part.

3DP is another process very similar to SLS. It also involves binding powder together, but a binding liquid is used to fuse the material together. A head similar to an inkjet printer

squirts binding agent in a computer-controlled path. Then the part lowers and more powder is swept over the top of it before the ink-jet head deposits the next layer. Many different polymers can be used in 3DP[6].

FDM is the most widespread and affordable type of additive manufacturing. The input material for FDM is a reel of filament. This filament is feed through the printer, where it is melted and extruded as a very thin thread or raster. The computer-controlled printing head deposits the material in continuous strands one layer at a time. Requirements for the feedstock material - must have melting or T_g temperature less than the max temperature of the print head. The unmelted filament acts as piston forcing material through the extruder nozzle. Because of the mechanics of FDM printing, the filament must not be too brittle and be strong enough to handle of the nozzle. The filament must be properly cooled to keep it from melting too far above the nozzle and buckling under the drive force. There are two standard sizes for filament, which require different hardware to print. The standard sizes are called 1.75mm and 3mm after the nominal diameter of each. Interestingly, the actual average diameter for 3 mm filament is 2.85 mm. High quality commercial filament keeps diameter tolerance around ±0.05mm. A FDM will have a larger range of diameters that it can print, varying with its design. More important than the exact diameter of the filament is the amount that its diameter varies. Substantial changes in filament diameter can affect the extrusion rate and reduce the geometrical accuracy. Thermoplastic materials are commonly used in commercial and consumer FDM printers. However some higher-temperature printers have been developed to print metals.

FDM printer are often equipped with two nozzles so that different materials or colors can combined in the same printing job. A common use of these nozzle is to have one head print support material is used to support overhanging material and other complex geometry, allowing difficult shapes to be printed easily. After printing, the support material is easily dissolved away, leaving only the part behind. Another use of this feature could be to insert supports of stronger material into a bulk part. This feature can cause difficulties if material leaks from the idle nozzle onto the part.

Another type of additive manufacturing has been developed based on FDM. Here the
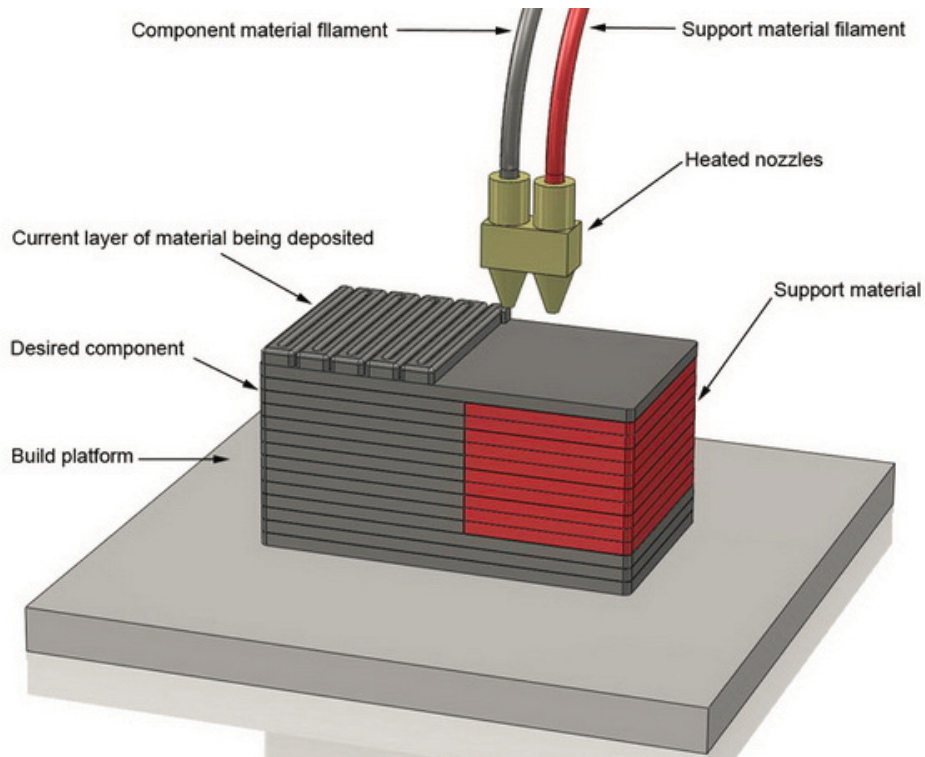
Figure 2.4: Diagram of FDM printing process. Figure copied from [7]

filament feedstock is replaced with a reservoir or syringe full of gel or ink-like liquid. The printer head moves around and deposits gel in a similar process as FDM printing. These types of printers based on this concept are generally smaller in scale and have tighter tolerances.

FDM printing is the most cost-effective and widespread form of 3D printing. This technology developed by S. Scott Crump in 1989. Crump founded Stratasys, Ltd. and patented the process, copyrighting the acronym FDM®to describe the process.[20] To avoid copyright infringement, other names such as Fused Filament fabrication (FFF) are sometimes used to describe this type of printing process.[20] A standard FDM printer has a maximum nozzle temperature of around 300 C Only materials with melting temperatures or glass transition temperatures (T_g) less than maximum temperature can be used in a printer. In practice, this means that FDM printing materials are limited to thermoplastics and thermoplastic composites. The most popular materials for FDM printing are Acrilonitrile Butadine Styrene (ABS), Polylactic Acid (PLA), and HIPS, which are all insulating materials.

A FDM printer has many processing parameters to be optimized to maximize the part

quality, strength, or cost. Each layer is extruded as a series of parallel lines called rasters. The bonding between the rasters is structural weak point. So, the printed material tends to be strongest in the direction parallel to the rasters. To contract this effect, most parts are printed so that adjacent layers have perpendicular rasters. Among the processing variations/parameters that could affect the parts properties are the following:

- Raster width: The thickness of the bead deposited by the nozzle.

- Air gap: the distance between the raster centers. Optimizing the distance between raster centers will create a stronger bond between the two adjacent rasters and therefore a stronger part. Usually a negative air gap is desired. Putting the rasters too close together will cause material to build up and ... A large air gap means that adjacent rasters will not bond together properly, and the material strength of the part will be compromised.

- Extrusion temperature: This is the temperature of the nozzle. Variations affect the viscosity of the extruded material. Too high of extrusion temperature causes material to leak out of the nozzle when it travels. This may result in threads of material stretching between different parts of the printed object. This can be counteracted somewhat by retracting the filament, so that material is farther away from the opening, but if too many retraction and extrusion cycles happen in a short time, the filament may be damaged, leading to a machine clog. If the extrusion temperature is too low, the material will not melt sufficiently and the extruder gears will not be able to push the filament through. The extrusion temperature may also impact how well the material bonds together.

- Bed temperature: Many FDM printers contain a heating element in the printing bed which heats its surface. The purpose of a heated bed is twofold. Firstly, it helps the first layer bond to the bed. If the first layer does not adhere to the bed, the part cannot be manufactured. ABS in particular is noted for not properly adhering if the print is unheated. Secondly, the heat from the bed, helps maintain an more even heat

throughout the part. If the heat is too uneven, the part will deform because the thermal expansion is significantly different in different parts of the material. This warping is permanent and remains after the part is removed from the print area. These effects are more prominent and problematic for large parts or parts with a long print time. Usually the temperature chosen for the bed temperature is around the glass transition temperature of the material being printed[20].

- Enclosure temperature: To further reduce the warping effects, high end printers have an enclosure around the print area. The air temperature with in the enclosure is controlled to prevent warping. Even in machines without an enclosure, the temperature of the air in the room and in the print area may affect the properties of the material.

- Layer thickness: The layer thickness is the height of each raster or layer. Thinner layers result in a part with better surface finish and vertical print resolution, but take much longer to print. Bigger layer heights are much faster. The layer thickness directly affects the final properties of the printed parts[20]

- Infill density and pattern: To conserve material, the interior of the part can be printed partially empty. The infill density is given as the percentage of the total volume occupied by printed material. Various patterns can be used to form a lattice in the infill space, some of which are better suited to higher or lower infill percentages. Reducing the infill density saves material and reduces processing time, but does decrease the material strength.

- Vertical and horizontal shell thickness: For parts printed at less than 100% infill density, there are boundary regions or shells on the outside surfaces of the part that are printed solid with no gaps. The thicknesses of these shells can be adjusted to an appropriate thickness for the part. Generally, the shell thickness of the top, bottom, and side surfaces are all independent. In Fig. 2.5 the solid perimeter visible around the infill is the horizontal shell.

- Printing speeds: The printing speed can affect the accuracy and surface quality of
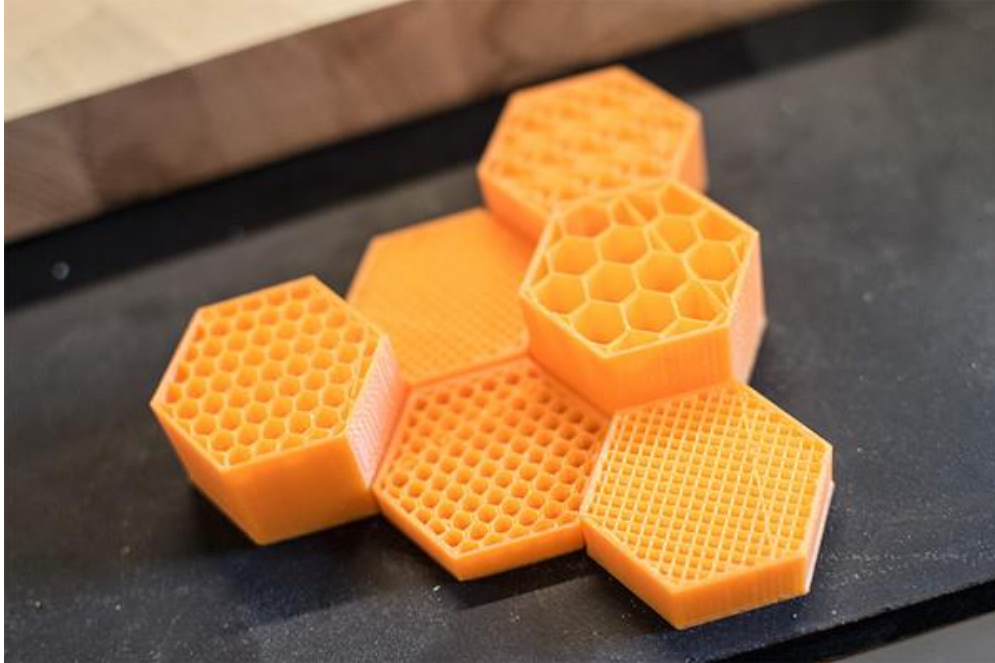
Figure 2.5: Picture showing various infill shapes and patterns. Figure copied from [8]

> printing, with slower speeds being more accurate. The back-pressure of the nozzle increases with higher printing speeds, causing the force required to extrude material to go up. This could cause problems if the filament is too weak or too soft. The advantage of higher printing speeds is the reduced time required to produce the part. The printing speed can be adjusted individually for different sections of the part such as the first layer, the last layer, the perimeters, the infill, and bridging material.

. Because the extruded plastic cools slightly before the next layer is printed over it, the inter-layer raster bonds are usually weaker than the intra-layer raster bond. So, the part will be weakest in the build direction, the direction in which the layers are deposited. Other factors affecting the mechanical properties include raster thickness, overlap of rasters, temperature of nozzle and printing bed, and speed of printing. Because of the many different factors involved, properties may vary somewhat between different models of FDM printer. Sometimes voids are planned in the interior of the part to reduced the material cost and printing time. Of course, this should be avoided when trying to maximize the strength of a part. Although researchers have studied the influence of these parameters on the material's

strength, the complicated interactions between the factors means that we do not yet have a unified picture of how each parameter affects the properties of a the final part.[20]

2.2 Composite Materials

One of the main challenges involved with additive manufacturing in general and FDM in particular is the small number of materials suitable for use in these process and the limited range of material properties available with these materials. A typical FDM printer can only reach 200-300 degrees C and so it is limited to printing thermoplastic materials. These materials have low strength and are thermal and electrical insulators. However, their properties can be greatly enhanced by mixing them together with other materials to form composites.

Composite materials are the mixture of two or more materials together in order to get a material with unique properties due to the interaction of the two materials. Usually, a matrix material that makes up the majority of the composite material and isl combined with a filler material with specially selected properties. The bulk material has properties that are a blend of the matrix material and the filler material. For example: to create a strong but lightweight material, you can mix a small fraction of strong and dense filler material into a lightweight resin or matrix. Such composites are often used in the aerospace and automotive industries due to the low weight and high strength of the material. Three common filler material shapes are long cylinders or wires, thin layers or sheets, and small particles. Cylinder and sheet-like materials can be short or extend all the way through the composite. Small cylinders and sheets of material can be aligned parallel to each other with a specific orientation or can have random orientations throughout the material. If the filler material has preferred orientation in one direction or plane more that others, the resulting composite material will have anisotropic properties. However, if the filler material is oriented randomly within the bulk material, that bulk material will have isotropic properties.
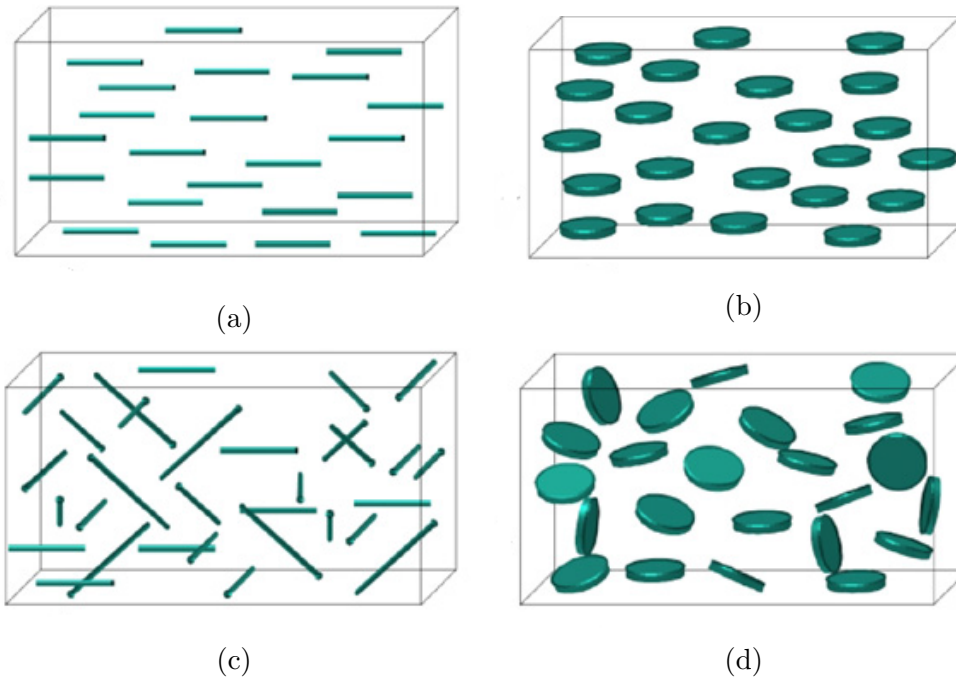
Figure 2.6: Diagram of composites with: (a) aligned fibers; (b) randomly oriented fibers; (c) aligned platelets; (d) randomly oriented platelets. Figure adapted from [9]

2.2.1 Composites and Mechanical Properties

Apart from the material properties of the independent composite materials and the concentration of filler material included, there are two other main factors affecting the mechanical properties of a given composite, Interfacial bonding and dispersion of filler material. Interfacial bonding is important to transfer the tensile properties of the filler material to the matrix[21;22] If the bonding between the matrix material and the filler material is weak.the materials will slide past each other rather than transferring the stress. When microscopy of a failure surface reveals fibers pulled out of the matrix, it indicates that poor interfacial bonding is the cause of the part failure. Additionally, when interfacial bonding is weak, the filler material behaves like a hole or flaw in the matrix material causing stress concentrations that weaken the material.[22] Poor filler dispersion in the matrix material also weakens the composite. In this scenario, filler materials clump together in agglomerations. Failure can occur if the bundle separates[22] or if the agglomeration causes stress concentration in the surrounding material.
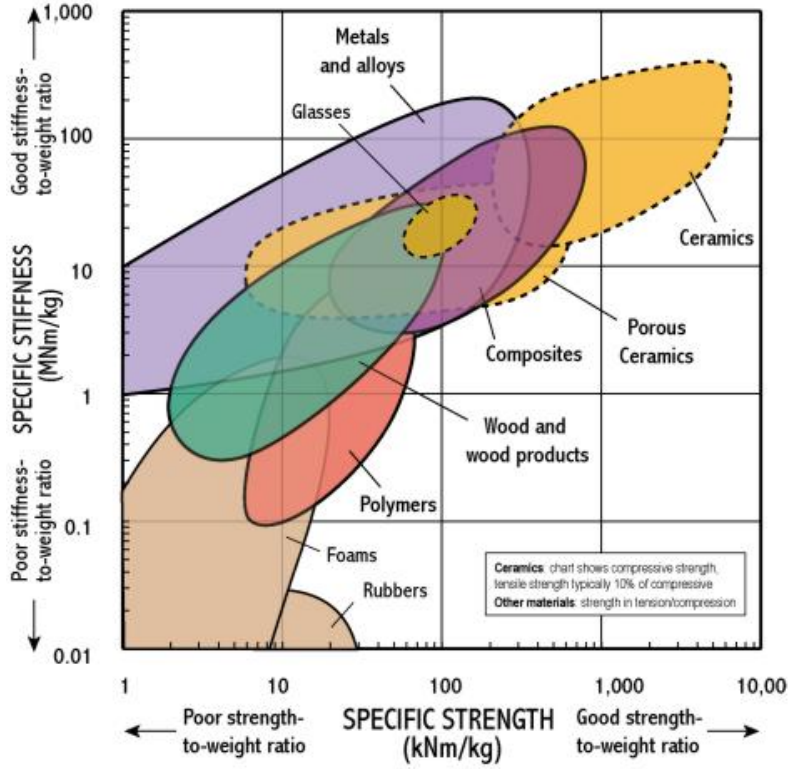
(a)
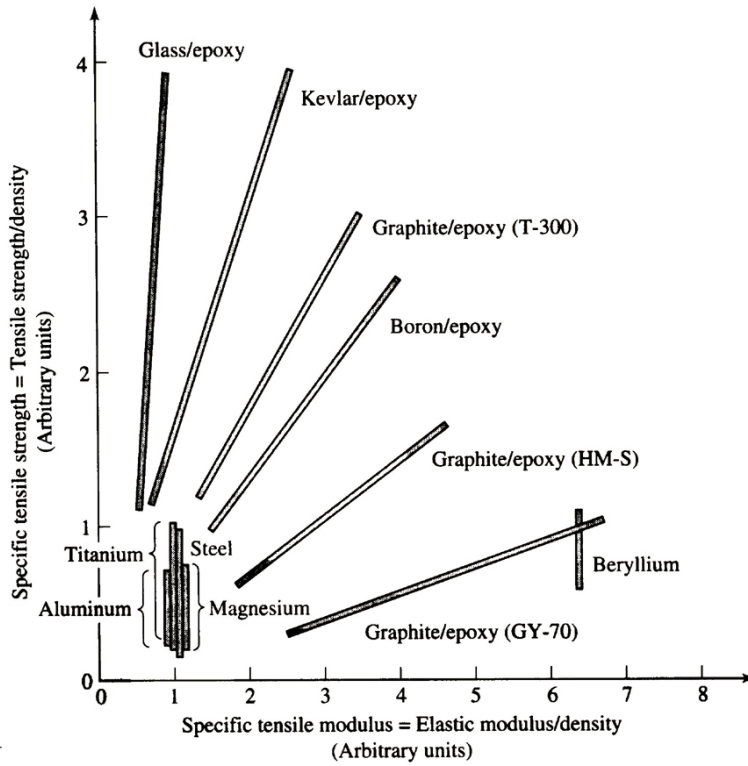
(b)

Figure 2.7: Composite materials' tensile properties compared with other materials (a) as general groups of materials (b) specific individual materials. Adapted from [10;11]

16
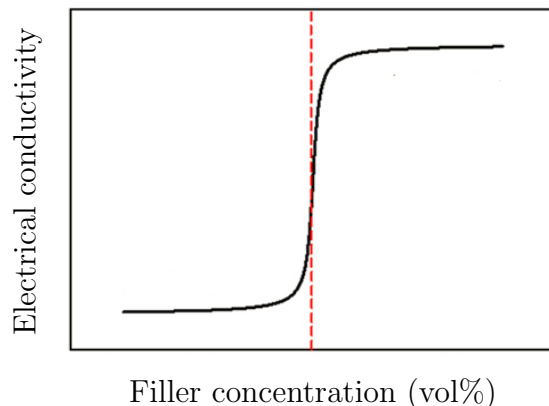
Figure 2.8: Graph of Electrical conductivity vs. filler concentration. The red dashed line is the percolation threshold. Adapted from [12]

2.2.2   Composites and Electrical Properties

The themoplastics are generally used in 3D printing are insulators. Adding a sufficient amount of conductive filler to a insulating matrix will improve the conductivity drastically. Percolation theory explains this transition from insulating to conducting. The conductivity is related to the weight or volume percentage of filler material in the composite.

Near a critical weight percentage called the peculation threshold, the conductivity of the composite undergos a major shift. At weight percentages below the threshold region, the filler materials are mostly insulated from each other by the matrix and the composite material has similar conductivity to the matrix material. The conductivity may increase slightly with increasing filler wt%, but will remain low until the percolation threshold is reached. Around the threshold region, the filler material concentration is sufficient to form a network of electrical pathways throughout the composite. Rather than being mostly separated by the insulating matrix, the filler particles are close enough to interact with each other. Note that filler materials do not necessarily need to be directly touching to form a conductive network. Electron tunneling can create a conductive pathway when conductive fillers are separated by about 10 nm or less[23]. At filler concentrations above the percolation threshold, the electrical conductivity of the composite may increase slightly with increasing filler loading. However, adding additional pathways quickly becomes redundant, and so has small effect.

Percolation theory has been adapted to model the electrical conductivity at varying filler
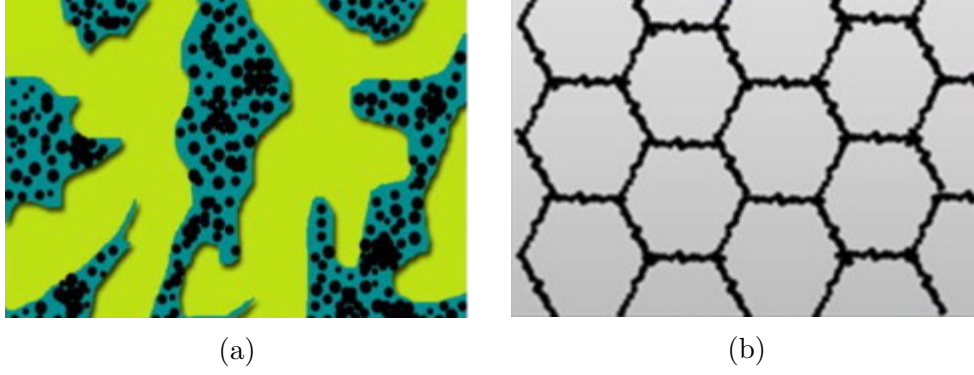
Figure 2.9: Diagram of concentrated filler material (a) in one of two immiscable polymers, and (b) at the interface between polymer granules. Adapted from [13;14]

loadings. Equation 2.1 is usually used[18]:

$$\sigma = \sigma_0(\phi - \phi_c)^t \, for \phi > \phi_c \tag{2.1}$$

Where σ is the specific conductivity in Siemens per meter (S/m), σ_0 is the proportionality constant in S/m, ϕ is the filler content in volume percentage, ϕ_c is the vol % of the percolation threshold, and t is the power constant. Theoretically, $t = 1.33$ for a two dimensional network and $t = 2.2$ for a three dimensional conductive network. However, experimentally determined values of t have not matched these values. Gao et al. created an in situ composite of ABS resin and graphene oxide with a percolation threshold of .13 vol % around which the composite transitioned from an insulator to a semi-conductor. At 2.33 vol % the composite had a conductivity of 0.1 S/m.[24]

The percolation threshold can be reduced by selectively increasing the concentration in certain portions of the composite over others. One method is to use a blend of two immiscable polymers, one of which dissolves the conductive filler better than the other. As shown in Fig. 2.9a, the filler will concentrate in the more favorable polymer. Because the unfavorable polymer takes up volume, the amount of filler needed to form a conductive network will be less than in a composite of just one polymer. As long as the high-filler concentration polymer extends through the material, the entire composite will be conductive. The percolation threshold will be the lowest at a specific ratio of favorable polymer to unfavorable polymer.

If too much of the unfavorable polymer is used, the other polymer will only be present in isolated pockets, which cannot connect to conduct throughout the material. For example, Taheri et al. studied the effect adding MWCNTs to blends of Polycarbonate (PC) and ABS, two immiable polymers. They varied the ratio of PC to ABS and found that MWCNTs were concentrated in the ABS portions of the polymer blend because MWCNTs have a greater affinity for ABS than PC.[25] A second method, which results in even lower percolation thresholds, isolates the filler material to the interface between polymer granules as shown in Fig. 2.9b. This is achieved by melt-compounding (see 2.4)two immiscible polymers or by compression molding polymer granules coated with filler materials.[14]

2.3   Nanomaterials

Nanomaterials are molecules or structures with at least one dimension in the range between one and several hundred nanometers. Fullerenes were the first discovered nanomaterial, discovered in 1985 by Harry Kroto, Richard Smalley, and Robert Curl[17]. Nanomaterials can be zero, one, or two dimensional. Zero dimensional nanomaterials have all dimensions on the nanoscale and are sometimes called quantum dots. One dimensional nanomaterials are constrained to the nanoscale in two directions, but can extend farther in the third directions. Examples are nano-wires, and nano-rods. Two dimensional nanomaterials have one dimension at the nanoscale, but extend farther in the other two directions, taking the form of a sheet or platelet. Grapene and Boron nitride are examples of two dimensional nanomaterials. Nanomaterials have great potential as filler materials for composites because of their high surface area per mass and large aspect ratios(for 1D and 2D materials).

Carbon nanotubes (CNT) one of the most popular and wide spread nanomaterials. They have been popularly studied and used since the discovery of Single-walled carbon nanotubes by ¡name¿ in 1991. CNT have a crystalline structure of carbon forming long tubes. The walls of the tubes are one atom thick in Single-Walled Carbon Nanotubes (SWCNT) and multiple layers thick in Multi-Walled Carbon nanotubes (MWCNT). SWCNT are more difficult and more expensive to produce than MWCNT As shown in Figure 2.10, SWCNT are have a
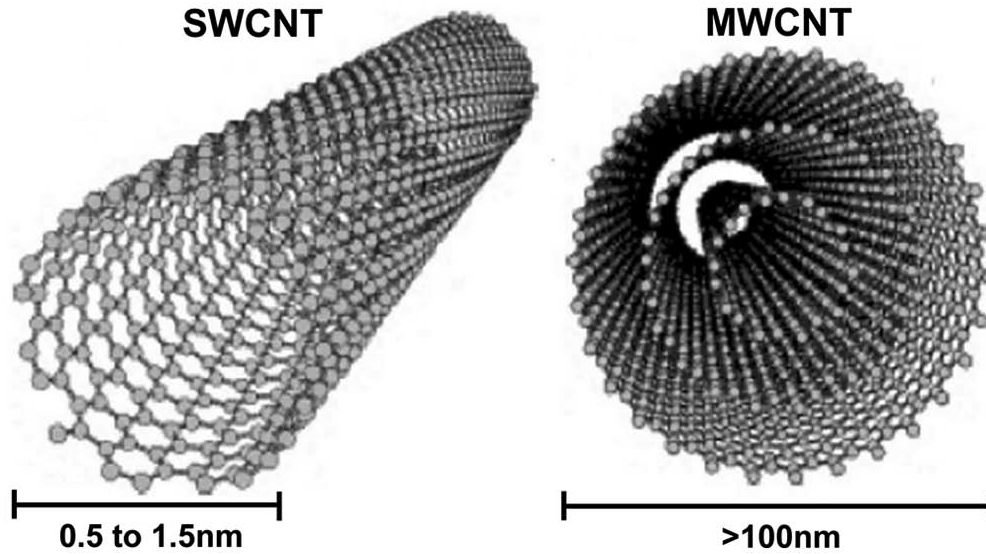
Figure 2.10: Schematic of Single-Wall and Multi-Wall Carbon Nantubes. Copied from [15]

diameter of around 1 nm while MWCNT have a larger diameters up to 100 nm. The length of CNT varies but can be up to a few μm. The gap between concentric wallls of MWCNT is fixed at 0.34nm.[26]. Weak Van der Walls forces attract CNT together, often forming clumps of CNT molecules. The interactions of CNT with other materials can be adjusted by attaching various functionalized groups to defects in the nanotube walls.These modified CNT are called functionalized CNT.

There are three major ways to manufacture CNT: laser ablation, arc discharge, and chemical vapor deposition (CVD). In laser ablation, a graphite block or target is placed in an inert atmosphere and heated to a high temperature. A laser pointed at the graphite vaporizes carbon from the block. Argon gas flow past the graphite target and carries the vaporized carbon downstream to a chilled collector. This collector cools the vaporized carbon which condenses on its surface in the form of CNT. Varying the temperature of the furnace and doping the graphite target with metals control the type and diameters of CNT produced. the In the arc discharge technique, two graphite electrodes are placed in an inert atmosphere. Creating an electric potential between them causes graphite to vaporize. The vaporized carbon deposits onto one of the electrodes, forming CNT. Different structures can be formed by varying the potential applied to the electrodes, and placing metal powder in the anode
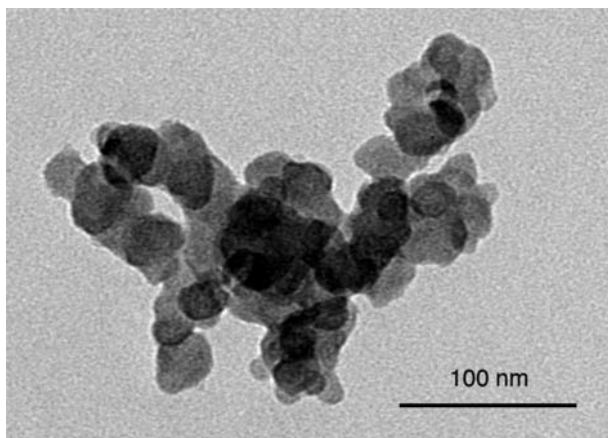
Figure 2.11: TEM image of Carbon Black. Copied from [16]

core helps control the thickness of the CNT. In CVD, a carbon based gas, such as methane, carbon monoxide or acetylene, is the source of carbon atoms rather than graphite. The gas is heated and pumped through a furnace maintained at a temperature in the range of 500-1200C. Because of the heat, the molecular bonds between the carbon and other atoms break, freeing the carbon atoms. Inside the furnace is a substrate coated with a transition metal which serves as a catalyst. Carbon crystallizes on the catalyst forming CNT. The unused gases exit the chamber, where they reform in to hydrogen and oxygen gas. The length of CNT is controlled by the reaction time. Other parameters are controlled by changing by varying temperature and other reaction parameters. By altering the parameters, CVD can also produce graphene or graphite. A common factor between all three methods is the difficulty of finding the correct process parameter required to create the CNT of a specific geometry.

The diameter and chirality of CNT determine their physical properties. While SWCNT may have either semiconducting or quasi-metallic behavior, MWCNT are usually semiconducting.[26] investigated the mechanical properties of individual arc-grown MWCNT (26-76 nm diameter) using Atomic Force Microscopy (AFM). They found the Young's moulus to be1.28 ± 0.59 GPa and the bending strength to be 14.2 ± 0.8 Gpa.

Carbon black consists of about 97% elemental carbon grouped into spheres. As shown in Figure 2.11, the spheres agglomerate together into groups of molecules with a shape

Table 2.1: Measured and theoretical properties of carbon fillers. Adapted from [18]

Property	Unit	Graphite	MWCNT	SWCNT	Graphene
Density	$g/(cm^{-3})$	~2.26	~1.8	0.8	~0.5
Elastic Modulus	TPa	~1 (in-plane)	0.3-1	~1	~1
Tensile Strength	GPa	~130	10-60	50-500	~130
Resistivity	$\mu\Omega * cm$	~50 (in-plane)	~5-50	~5-50	~1
Thermal Conductivity	$W/(m * K)$	~3000 (in-plane) ~6 (z-axis)	3000(theoretical)	3000 (theoretical)	~5500

similar to bunches of grapes. Carbon black is synthesized by burning carbon compounds in a controlled procedure. It is a common component in tire rubber and is fairly inexpensive to produce.

Graphene and Graphite are related forms of carbon material. When carbon atoms connect in a 2D sheet-like hexagonal lattice, they form the nanomaterial graphene, the first known material of single atom thickness. Graphene was first isolated by Novoselov et al. in 2004. They produced it using a mechanical exfoliation process, but it can also be manufactured using CVD or by chemically separating graphite using Hummer's method. When van der Waals forces join multiple layers of graphene together, the bonded layers form graphite, a common naturally occurring form of carbon. Graphite can be considered a nanomaterial when its thickness is less than 100nm, but most graphite exists in crystals larger than the nanoscale. CNT, carbon black, grapene and other nanomaterials have been previously been shown to improve many properties of thermosets and thermoplastics.

2.4 Methods of Synthesizing Polymer Nanocomposites

There are several methods of creating polymer composites with nanofillers. When creating nano-composites a common problem is agglomeration, or clumping, of nanoparticles. Attractions between the nano-particles can keep them from dispersing evenly in the polymer mixture. This reduces the ability of the nanomaterial to form a network, and inflates the percolation threshold. Agglomerations of nano-materials can cause stress concentrations in the surrounding plastic, weakening the the mechanical strength of the composite material. So, when creating a polymer-nanomaterial composite good dispersion of the nanomaterial is

desired. The most common methods of making nanocomposites with thermoplastic matricies are *in situ* polymerization, solution mixing, and melt compounding.[27]

In situ polymerization is a technique where the polymer is synthesized in the presence of the desired fillers. First, monomer or small polymer molecules are mixed together with the right concentration of polymers. Through controlled reactions, the polymer grows around the nanomaterials. Composites formed by this method tend to have stronger interactions between the polymer and fillers than those formed by the solution mixing or melt-blending. In addition, filler materials disperse better resulting in lower percolation thresholds. However, this method requires a large amount of electrical energy to disperse the filler material during the polymerization process.[18]

In solution mixing, the polymer is dissolved into a solvent and an appropriate amount of nanomaterials are added to the solution. A mechanical mixing method, such as sonication or magnetic mixing, disperses the fillers in the solution. After good dispersion is achieved, the solvent is evaporated away leaving the composite material behind. The polymer formed in solution mixing or *in situ* polymerization can be molded or otherwise processed to the final shape required. In a variation of the solution mixing technique, the solution is electrospun before the solvent evaporates. During electrospinning, a liquid solution or melted polymer is fed through a spinneret, which is typically a hypodermic syringe needle. Strong electric charges at the needle tip force the material to be extruded in thin nano-scale threads. These threads make up the desired composite material.

During melt-compounding, the polymer is heated above its glass transition temperature (T_g). Nanomaterials are added, and the mixture is mixed to achieve good dispersion. Extrusion is a form of melt compounding because both single screw and twin-screw extruders mix the materials in the heated region. Another common machine used for melt compounding is the compounder. A compounder melts the polymer and shears the composite mixture until constant torque is reached. Because more mixing occurs in a compounder than in and extruder, compounders usually achieve better dispersion. After compounding, the composite material can be extruded or molded to the desired shape. Melt-compounding methods use types of machines common in industrial applications, and so scale up very easily. However,

23

the shear forces involved can damage the nanomaterials which reduces their effectiveness. Solution mixing can also damage the filler materials. Polymer made with melt-compounding technique usually have higher percolation thresholds compared to those made using other methods[14]. Higher percolation threshold has been associated with high melt viscosities and reduced ductility and toughness[14] So, while melt-compounding is the most favorable technique for industrial applications, it is not without is drawbacks. Since FDM printers use filament as feedstock material, polymer composites used in 3D printing use extrusion as the final step regardless of the synthesis process employed.

2.5   Composite Materials in Additive Manufacturing

Because potential for improving the properties of 3D printed polymers by adding fillers, researchers have begun investigating the effectiveness of various additives. Several composite technologies like continuous fiber reinforcement using carbon fiber in a nylon matrix or CNT composite filament have already been developed in the industrial field, but the effect of these improvements has not been thoroughly studied. For FDM type 3D printers, Perez et al mixed ABS with 5 wt% of jute fibers, Thermoplastic Elastomer (TPE), and Titanium Oxide (TiO_2). They found that the addition of TPE reduced the anisotropy of the material. The 5 wt% TiO_2 increased the ultimate tensile strength by 13.2% and 30% in directions perpendicular and parallel to build height respectively.[28] Tekinalp et. al studied the ABS composites reinforced with up to 40 wt% of short carbon fibers and achieved significant mechanical enhancement. The tensile strength increased 115% and the elastic modulus increased 700%. They compared FDM printed composites with compression molded composites and found that the FDM printed composites had greater fiber alignment than the compression molded.They also found the fiber length was significantly shorter in the composite than it was originally, probably because it was damaged during compounding.[29] Researchers have started to explore the effect of nanoscale additives. In 2003, Shofner et al. formed a composite material out of vaper grown carbon fibers and ABS. They were able to improve the tensile strength by 24.4 MPa or 29%[30] Later, Shofner continued his research and

made a 5 wt% ABS-SWCNT composite. His team used a modified apparatus to print it in a method very similar to FDM printing, however the feedstock material was cast bars rather than filament. The resulting printed material had a 26% increase in tensile modulus, but no improvement in tensile strength. The composite feedstock material was 31% stronger than the neat ABS composite. Poor interfacial bonding during the printing process was cited as the reason that the material didn't retain its advantages after printing.[31] Around the same time, Ou et al. studied the percolation of carbon black in ABS filament fabricated using a melt-compounding method. They found the percolation threshold to be around 10 vol%[32] Tsiakatouras et al. found that the elastic modulus of FDM printed ABS increased with the inclusion of 0.5-3% CNT. With the addition of embedded carbon fibers, elastic modulus increased even more[33]. However, they did report the tensile strength or electrical properties of their composite material. More recently, in 2015, Wei et al mixed Graphene oxide and ABS by solvent mixing in a N-Methylpyrolidone(NMP) solution. After mixing, they reduced the Grapene oxide to graphene using hydrazine hydrate, and precipitated out the NMP using water, formming Graphene-ABS coagulations. These precipitates were separated out and extruded to form feedstock filaments of up to 7.4 wt% grapene. The electrical percolation threshold was found to be around 2.0 wt% or 0.9 vol%[34]

Chapter 3

Methods

This chapter details the materials, equipment, and procedures used to manufacture and test composite materials. First the materials used are described, then the process of making 3D composite materials is explained. Next, the procedures for the material characterization tests are explained. Finally, tensile and electrical testing procedures are discussed.

3.1   Materials

ABS composite materials were created using grade ABS448T ABS plastic from Star Plastics, Inc.(Millwood, West Virginia) that was purchased through Filabot (Barre, Vermont). Four types of carbon filler materials were used: Graphite, CB, MWCNT, and SWCNT. The graphite flakes (Sigma-Aldrich, St. Louis, Missouri) used were sized so that 75% of the material was lager than 100 mesh. This mesh has openings with a nominal size of 0.149 mm. Prior to use, this graphite was ground in a mortar and pestle for 10 min to reduce the flake size. MWCNT were provided by Bayer Material Science AG, Leverkusen, Germany and had 3-15 walls, 3-20nm outer diameter, and $> 1\mu$m length. SWCNT were provided by the National Institute of Standards and Testing (NIST) in Boulder, Colorado and had a diameter of 1-2 nm. CB particles are typically sold as 80-800 nm aggregates clumped together in agglomerates with a size of 0.1 to several micrometers.
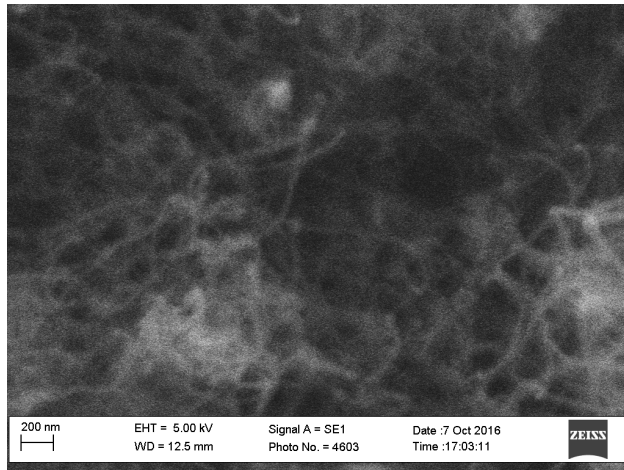
Figure 3.1: SEM image of Baytubes MWCNT

3.2   Filament Extrusion

The first step in manufacturing the FDM printed composite specimens is making composite filament for input into the printer. First, the carbon nanomaterial is weighed and mixed with ABS pellets. Weights are controlled to make the desired weight percentage. After mixing, the composite mixture was extruded though a Filabot Wee (Barre, Vermont) single-screw extruder with a screw speed of 43 RPM. The plastic expands after extrusion so the die must be smaller than the desired filament. A circular die with a hole diameter of 2.15 mm was used to extrude filament with a diameter of 2.85 mm. The addition of filler material changes the thermal properties of the plastic, so slightly higher temperatures were needed to maintain the same diameter of filament at higher loadings. The typical temperature range was between 192°C to 204°C. Placing a fan near the die helps control the cooling rate of the filament and reduces distortion of the hot, softened filament. Figure 3.2 shows the extruder used and provides a schematic of the extrusion process. ABS pellets enter the machine from through the hopper in the top of the machine. Gravity forces the material into the screw drive. A DC motor turns the screw drive forcing the materials into a heater where the ABS is melted. The rotation of the screw drive mixes the filler material and ABS together. Finally the melted mixture passes through the die and emerges from the extruder in a continuous filament.
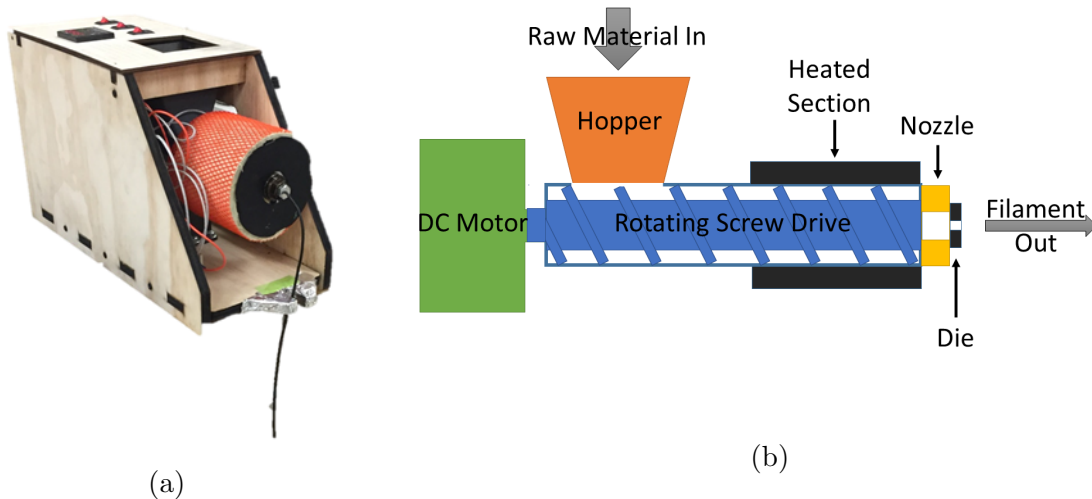
Figure 3.2: (a) Picture of Filabot Wee extruder, and (b) Diagram of extruder components

3.3 3D Printing

A Lulzbot Mini (Aleph Objects, Inc., Loveland, Colorado) printed specimens for tensile testing and Electrochemical Impedence Spectroscopy (EIS). Cura Lulzbot Edtition 18.03 software was used as the slicing engine. The 0.5 wt% carbon black tensile ASTM D638-14 Type IV specimens were printed using a Airwolf 3DHD (Airwolf 3D printers, Costa Mesa, California) printer with MatterControl 1.2 software. Processing parameters used in the printing process are shown in Table3.1. Different printing settings were required for 15 wt% MWCNT filament to avoid clogging. The setting changes made reduce the back pressure of the nozzle, putting less strain on the extrusion gear. The filament we produced varied in diameter from batch to batch and along its length, so the filament diameter setting was set to the average diameter of the filament being used. This variation in diameter was partially due to changing pressure in the extruder as the hopper emptied.

Tensile test specimens were manufactured to meet ASTM D638-14 Type IV or Type V specimen standards.The majority of specimens were Type IV and had the dimensions shown Figure 3.3b. Figure 3.3c compares the relative sizes of Type IV and Type V specimens. Part rasters were oriented at 45° from the loading direction with layers perpendicular to the the part thickness.

(a)

Raster
Directions

R = 25 mm

1 Perimeter

19 mm

6 mm

R = 14 mm

25 mm

155 mm
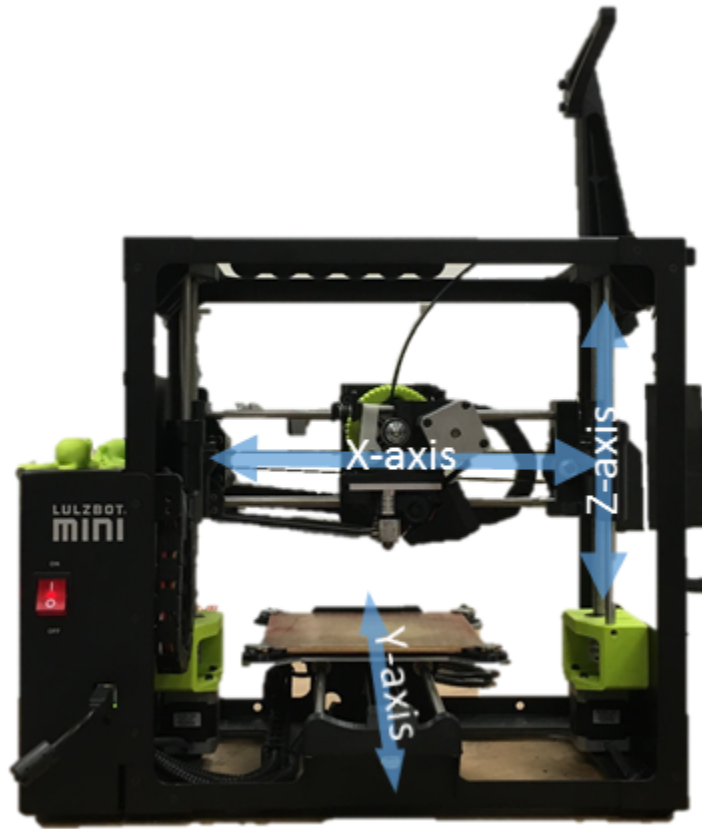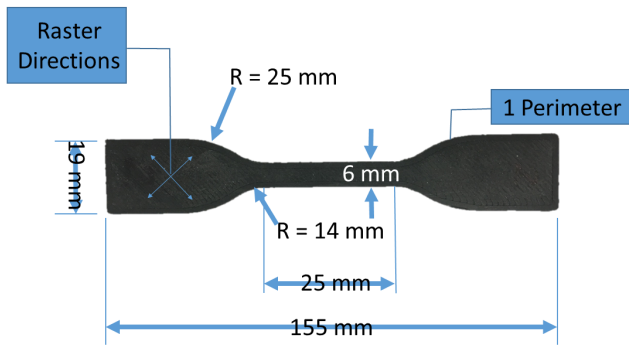
(b)

(c)

Figure 3.3: (a) Lulzbot Mini: DC motors are used to control the position of the extruder in along 3 axes; Tensile test specimens (b) manufacturing parameters and dimensions of ASTM D638-14 Type IV specimen (c)Comparison of Type IV and Type V specimens

Table 3.1: Selected 3D printing settings for tensile test specimens

Parameter	General	15 wt% MWCNT
Nozzle Size	0.5 mm	same
Layer Height	0.21 mm	0.25 mm
Shell Thickness	0.45 mm	same
Infill Density	100%	same
Print speed	30 mm/s	20 mm/s
First layer thickness	.42 mm	0 mm
First layer print speed	15 mm/s	10 mm/s
Travel speed	175 mm/s	same
Printing temperature	240°C	255 °C
Bed temperature	115°C	same
Filament Diameter	varies	varies

Most tensile specimens were tested as printed. As detailed in Chapter 3 , some specimens received post-printing heat treatment according to the following procedure: Microwaved specimens were microwaved in a Nitrogen atmosphere in a 900 Watt Emerson household microwave for 3 seconds. Oven heated specimens were placed in an oven heated to 135°C for 1 hour. MWCNT oven specimens were microwaved prior to being placed in the oven, while neat ABS specimens were placed directly in the oven.

The Lulzbot printer was used to print specimens for EIS. These specimens were 1 cm diameter disks 100 microns thick. The general settings shown in Table 3.1 were used except for the layer height which was reduced to 100 microns.The result was a one layer thick disk of 3D printed composite. These disks were also used to collect XRD and Raman spectra.

3.4 Material Characterization

3.4.1 Thermogravimetric Analysis (TGA)

TGA was conducted at NIST using a TG 209 F1 Libra(NETZSCH, Selb, Germany). Powdered Graphite, MWCNT, and CB were tested as well as chopped fragments of filament. TGA was conducted in an air atmosphere with a temperature range from 30° to 800°. Temperature increased at a rate of 10° per minute. Three samples of each material were tested.

3.4.2   Raman Spectroscopy

Raman spectroscopy was conducted on 100 micron thick samples of 3D printed material. Nanomaterial samples were powders mounted on a glass slide. A LabRAM ARMIS (HORIBA Jobin Yvon, Edison, New Jersey) operated by the Bioengineering Research Center, University of Kansas, Lawrence, Kansas was used to collect the data.

3.4.3   X-Ray Diffraction

XRD was carried out using a Panalytical Empyrean(Almelo, Netherlands) X-ray Diffractometer with a Cu target X-ray source and a 45 kV and 40mA power output. The sample stage rotated at 1/4 rev/sec. On the incident beam side a 0.04 rad soller slit was used, and on the diffracted beam side was a 0.02 rad soller slit with a PIXcel3D medipix3 1x1 detector. Powdered samples of graphite and MWCNT were analyzed along with 3D-printed samples of composite plastics. Powdered MWCNT and Graphite samples were placed in a 27mm sample holder and compacted to form as flat a surface as possible as shown in Figure 3.4. The XRD used a divergent slit set to an irradiated length of 20 mm, a 15 mm mask, and an anti-scatter slit of 4 degrees. 3D printed composite samples were 1 cm disks with 0.1mm thickness. Samples tested were 5 wt% MWCNT and 1 wt% Graphite. They were placed on a zero background detector. For these composite samples, the divergent slit was fixed at 1/8 degrees with an anti-scatter slit size of 1/4 degrees and a 10 mm mask.

3.5   Tensile Testing

Tensile tests were conducted with a Shimadzu (Kyoto, Japan) EZ-LX and TrapeziumX software with a 5 kN load cell at a 5 mm/min crosshead speed and 65 mm initial crosshead separation. An Epsilon(Jackson, Wyoming) Model 3542 extensometer with 50mm gage length coupled with a a Shimadzu ESA-CU200 external sensor amplifier collected precise strain data throughout the tensile test. Due to variations in the specimen dimensions, the crossection of each individual test specimen measured before tensile testing. Five measure-
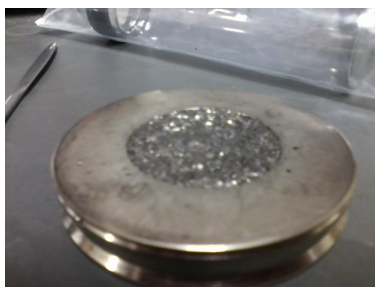
(a)

(b)

Figure 3.4: XRD setup (a) graphite powder in sample holder (b) XRD X-ray source, sample stage and detector.
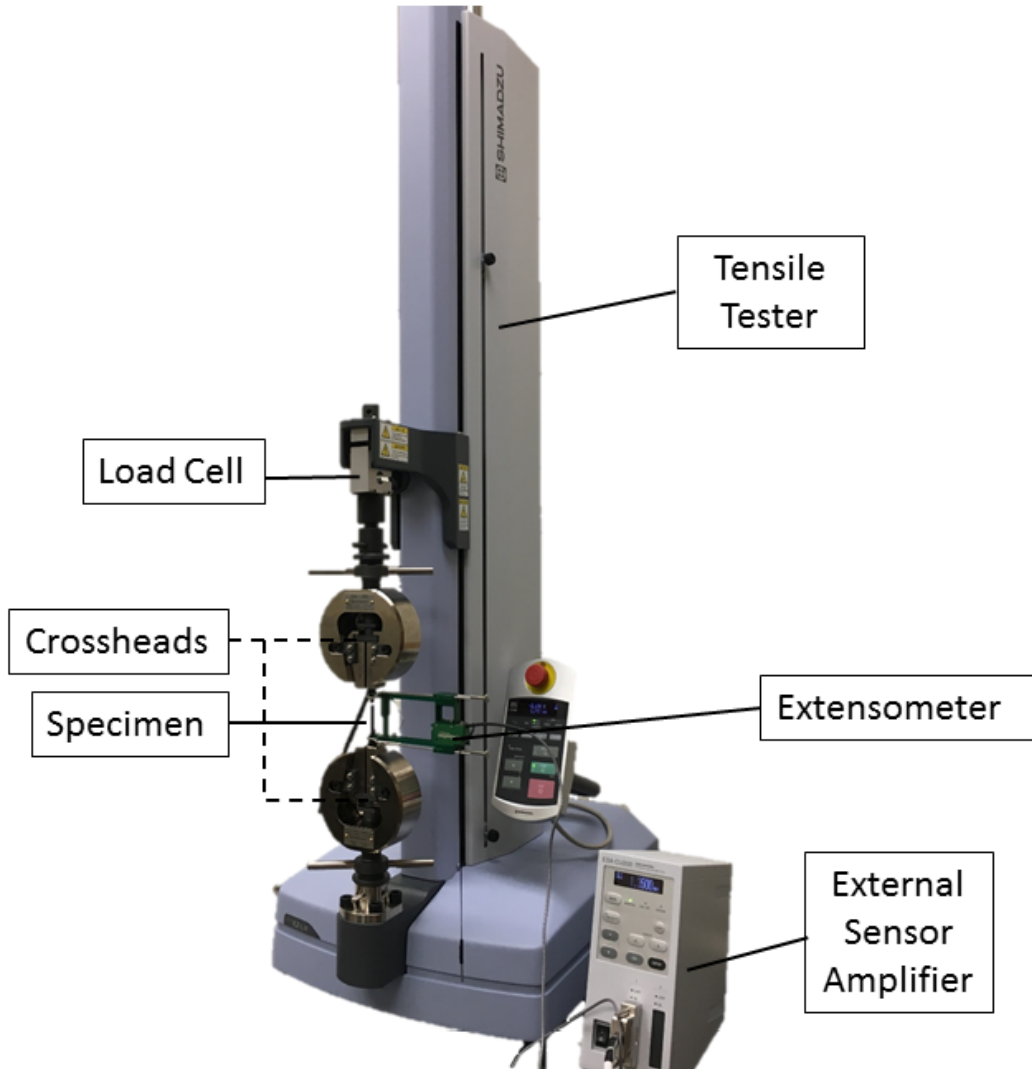
Figure 3.5: Type IV sample mounted in EZ-LZ with extensometer attached

ments were taken at three locations along the gage section and averaged together to find each crossectional dimension. A few subsequent tests were conducted using ASTM D638-14 Type V specimens at a 1 mm/min crosshead speed with a 25.4 mm initial crosshead seperation. For these tests the initial crosshead separation was 25.4 mm and strain was calculated from the crosshead displacement.

(a)   (b)

(c)
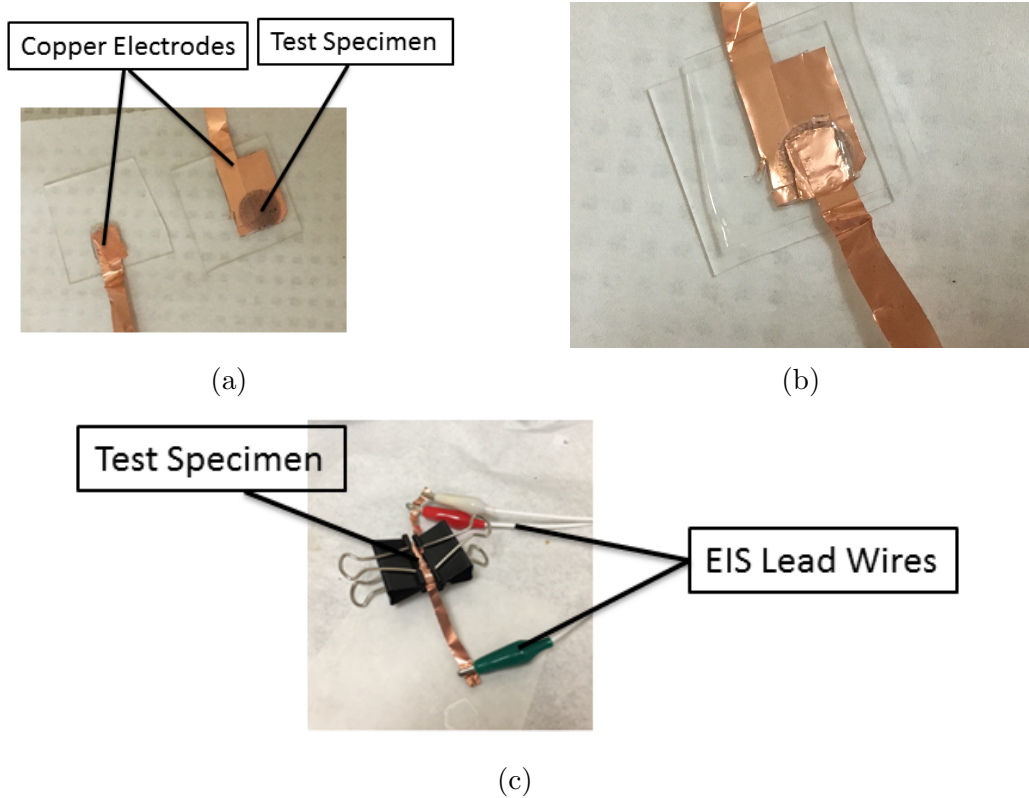
Figure 3.6: Preparation of EIS samples (a) Sample disk placed on foil (b) disk sandwiched between foil (c) setup connected to Electrochemical workstation

3.6   Electrochemical Impedance Spectroscopy

Thin disks were manufactured using EIS. After manufacturing, the disks were mounted between between two pieces of copper foil. These foil pieces were sandwiched between two glass slides, and pressure was applied to hold the setup together as shown in Figure 3.6.

A CHI 660E Electrochemical Workstation (CH intruments, Inc., Austin, Texas) was used to conduct electrical impedance tests. Electrical Impedence Spectroscopy(EIS) of the samples was conducted from 1 MHz to 100mHz with 20 mA voltage.

3.7   Fracture Surface Imaging

Images of the fracture surfaces of the tensile test specimens were taken with a optical microscope and a Scanning Electron Microscope(SEM). An 1/4-1/2 in long piece of the gage

Figure 3.7: Leica DVM2500 digital Microscope

section containing the fracture surface was separated from the broken specimens using a razor. This sample was mounted and imaged with the fracture surface perpendicular to the incident beam. A Carl Zeiss(Jena, Germany) EVO MA10 Scanning Electron Microscope (SEM) system with a SmartSEM software suite captured images of the fracture surfaces of the dogbones.

Additional images of the fracture surface were gathered using a Leica (Wetzlar, Germany) DVM2500 digital microscope with a VZ 700 C zoom lens. Samples were mounted glass slides using clear tape.

Chapter 4

Material Composition

After producing filament and 3D printed composite material, I verified the composition of the material through XRD, Raman, and TGA.

4.1 X-ray Diffraction

X-ray Diffraction is a material characterization technique used for crystalline materials. It measures the distance between crystal planes. These distances can be used to identify unknown materials or the structure of known materials. Diffraction is a physical phenomena that occurs when a wave interferes with interferes with itself after passing through a barrier. When a wave passes through a single slit that is slightly larger than its wavelength, it interferes with itself forming patterns of constructive and destructive interference. After, interference the intensity of the light depends its angle relative to the incident.

X-ray light has wavelengths similar to the lattice distances in crystals. When X-rays are incident on a crystalline material, the reflections from a similar diffraction pattern to double and single slits experiments. These diffracted X-Rays form intense peaks at different distances from the crystal. XRD records the intensity of X-Rays at various angles from the sample surface. Peaks in intensity can be attributed to different crystal faces of the unit cell. The d-spacing between the crystal planes can be estimated using Bragg's Law:

$$d = \frac{\lambda}{2sin(\theta)} \tag{4.1}$$

Powders of randomly ordered crystals diffract X-rays into of a circle of high intensity X-rays that is centered around the direction of the incident light. However, a single crystal or highly aligned crystals will diffract X-rays only into one single direction. These reflections may be missed by the detector, which only captures a small segment of the cone. For this reason powdered specimens are the preferred specimens for XRD. Single crystals or highly aligned crystals such as carbon nanotube forests are more difficult to detect. Monochromatic X-rays are preferred for XRD tests, because any uncertainty in wavelength results in uncertainty in d-spacing.

In XRD tests, the graphite powder showed a strong peak at 26.6 °2θ as shown in Figure 4.1a. This peak is well known to be the (002) peak of graphite and corresponds to the interlayer distance. From the (002) peak, the d-spacing is calculated to be 3.34 Å. This value matches the interlaying spacing of graphite, 3.34 Å, confirming its crystalline structure. Since CNT have a graphitic structure, we expect a similar profile for them. Figure 4.1b shows the result of the XRD tests for MWCNT. This sample has a broad peak centered at 25.9 °2θ. Using Braggs law, the d-spacing of nanotubes is calculated to be centered at 3.44 Å. This interlayer distance is the same as that of turbostratic carbon. Turbostratic carbon is similar in structure to graphite, consisting of stacked layers of graphene. However, in graphite the graphene layers have an ABAB stacking structure where the carbon atoms in A sheets are vertically aligned with each other. The atoms in the B sheets are also vertically aligned with each other and offset so that there is an atom in the center of each A sheet ring. This alternating sheet crystal forms a very stable structure. In turbostratic carbon, the graphene layers are rotated and translated away from the graphite structure resulting in a random positioning of atoms in one sheet relative to atoms in another sheet. These deviations from graphites structure are accompanied by an increase in interlayer distance[35]. This XRD data indicates that the shells of the MWCNT are not aligned in a perfect graphite structure, but have a turbostratic structure. This increased interlayer spacing is commonly found in
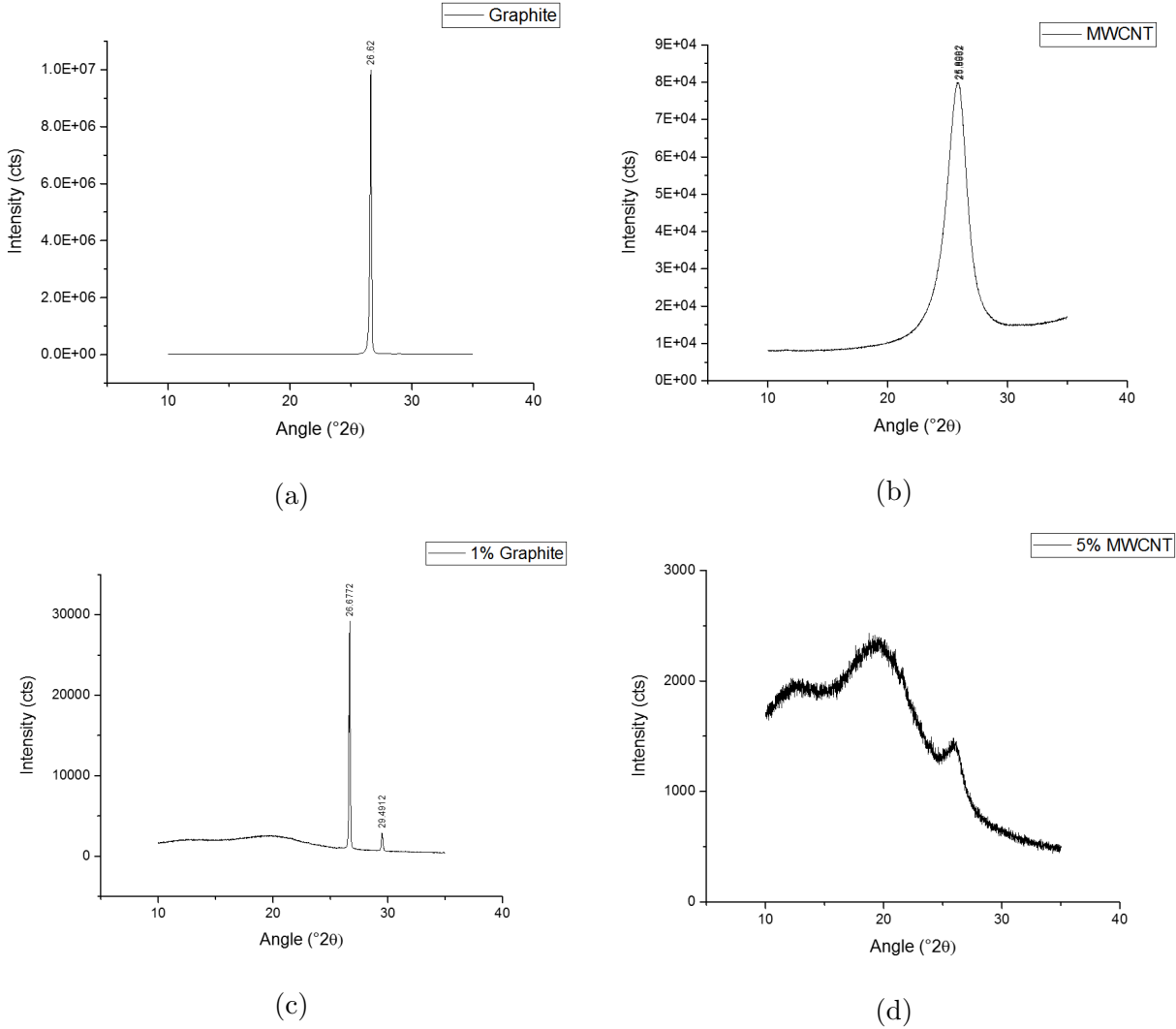
Figure 4.1: XRD data for (a) graphite powder (b) MWCNT powder (c) 1.0% Graphite/ABS composite (d)5.0% MWCNT/ABS composite

CNT[36].

The MWCNT (002) peak is weaker and broader than the graphite peak. This broadening effect is caused by two major factors strain broadening and domain size broadening. Turbostratic carbon has a random distribution of interlayer spacings, and each corresponds to a slightly different angle. In addition the interlayer spacing decreases as the diameter of the graphene shells increase, causing a natural broadening of the peak[36;37] Broadening of the peak due to a variety of interlayer spacings is called strain broadening.

The small size of carbon nanotube also contributes to peak broadening. Crystals under

100 nm in size cause peak broadening in XRD. This effect is known as size broadening.

The graphite composite showed strong (002) peak at 26.7 °2θ and a weak peak at 29.5 °2θ. These peaks correspond to d-spacings of 3.34 Åand 3.02 Årespectively. From this we can conclude that XRD is detecting the graphite in the composite specimen. The MWCNT composite specimen has very weak signal similar to an amorphous specimen. There is a slight increase in signal intensity near 26 °2θ, that probably corresponds to the presence of MWCNT in the specimen. As the signal is very weak, it could conceivably be part of the background noise rather than due to the presence of MWCNT.

4.2 Raman Spectroscopy

Raman spectroscopy is useful for identifying and differentiating between carbon materials. The unique structure of each material produces characteristic peaks, which identify the material. During Raman spectroscopy, a single frequency laser is directed at the test specimen, some of the light will interacts with the material and is scattered. Most of the scattered light is at the same frequency as the incident light, but a small portion of it will be at other frequencies. This light scattered at a new frequency is known as Raman scattering, or inelastic scattering, and light scattering at the original frequency is called Rayleigh scattering, or elastic scattering. By detecting the intensity and frequency of the Raman scattering, the material can be identified. Raman scattering can be analyzed both by classical theory, which considers light to be a wave, and by quantum theory, which considers light to be a stream of photons.

In classical theory, light is considered to be an electromagnetic wave. As it reaches a molecule, the electric portion of the wave induces a fluctuating dipole moment on the molecule. The strength can be mathematically described as,

$$P = \alpha E \tag{4.2}$$

where P is the strength of the dipole moment, α is the polarizability of the molecule, and E

is the strength of the electric field induced by light. Since light is wave, E varies with time according to the formula:

$$E = E_0 cos(2\pi\nu_0 t) \tag{4.3}$$

Where E_0 is the amplitude of the electromagnetic wave, ν_0 is the frequency of the incident light, and t is time. Equation 4.3 is a general formula for any light wave. The polarizabiliy of the molecule is a measure of how easily a molecule is polarized and depends on many factors such as the size and shape of the molecule, as well as the type of bonds holding the molecule together. The polarizablity can also be affected by the movement of the molecule. For a small movement dQ, we can consider the polarizabilty to be

$$\alpha = \alpha_0 + (\frac{\delta\alpha}{\delta Q})_0 * dQ \tag{4.4}$$

where α_0 is the polarizabilty at some equilibrium position. dQ is the displacement, and $(\frac{\delta\alpha}{\delta Q})_0$ is the rate of change of polarizability with respect to molecular position. The small displacement dQ is caused by vibration of the molecule, which occurs at a frequency ν_m, and can be modeled as

$$dQ = Q_0 cos(2\pi\nu_m t) \tag{4.5}$$

where Q_0 is the amplitude of molecular movement. By combining Eqns. 4.2-4.5, we find the strength of the dipole to be

$$P = \alpha_0 E_0 cos(2\pi\nu_0 t) + \frac{1}{2}(\frac{\delta\alpha}{\delta Q})_0 Q_0 E_0 [cos(2\pi(\nu_0 + \nu_m)t)cos((\nu_0 - \nu_m)t)] \tag{4.6}$$

This oscillating dipole in turn produces light waves. The first term has the same frequency as the incident electromagnetic wave and represents the Rayleigh scattering. The second term represents both the Stokes and anti-Stokes Raman scattering, and is considered to be due to the vibration of the molecule. Note that Raman scattering only occurs if the polarizability of the molecule changes with respect to molecular position. So, Raman scattering only occurs when molecular vibrations affect the polarizability of the molecule.
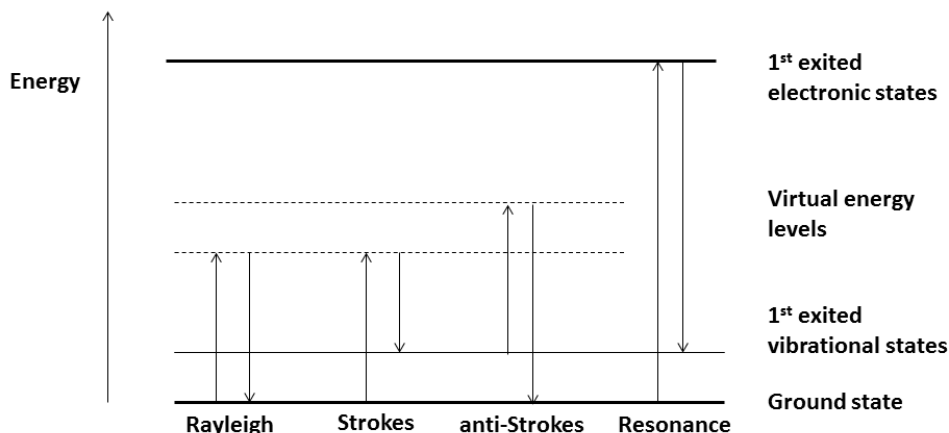
Figure 4.2: Diagram of Rayleigh, Stokes, anti-Stokes and resonance processes. Copied from [17]

Raman scattering can also be analyzed from a quantum mechanics standpoint, where light is modeled as a stream of photons rather than a electromagnetic wave. The photon carries a fixed energy determined by its frequency. At the same time, each type of molecular has discrete energy levels. A molecule with excess energy will emit photons to return to a stable molecular energy level. For example, in Rayleigh scattering, a molecule absorbs a photon of light and moves to a higher energy state. Because the higher energy level is unstable, the molecule returns to the original energy state and emits a photon. The frequency of the photon is determined by its energy, and the same amount of energy enters and leaves the molecule. So, the frequency of the incident and scattered light is the same, and it is Rayleigh scattering.

However in Raman scattering processes, the molecule emits a different energy photon than the one it absorbs. In the Stokes scatter process, a photon raises the molecule to a higher energy level. However, rather than returning to the original state, the molecule returns to a intermediate stable energy state as shown in Figure 4.2. As the molecules energy lowers, it emits a photon with a smaller energy and frequency than the incident photon. In anti-Stokes scattering, the molecule starts at an exited state, absorbs a photon, and transitions to a higher energy level. Then the molecule emits a higher energy photon and falls down to a lower energy state than the initial energy state. So, by quantum theory, Raman scattering

41
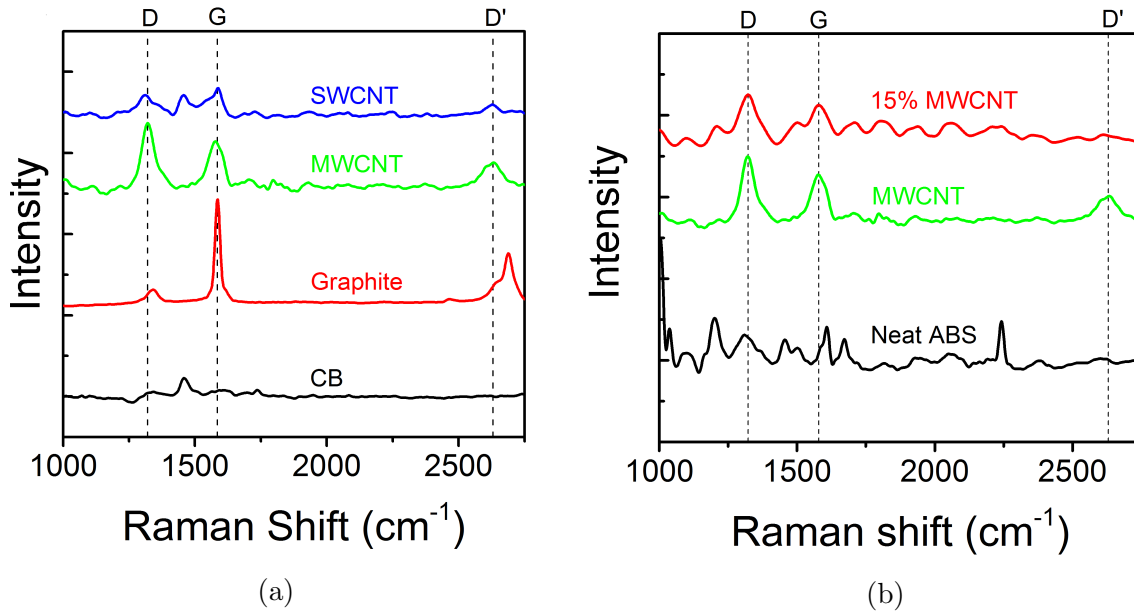
Figure 4.3: Raman Spectra of a)Carbon fillers and b)MWCNT powder, 15% MWCNT/ABS composite and neat ABS sample

is modeled as photons emitted at different energies than they are absorbed due to molecular energy changes.

The Raman spectrum of MWCNT shares two bands with Graphite, because they have the same basic hexagonal molecular structure. The G band at is near 1580 cm^{-1}, which is caused by in-plane vibration of the C–C bond. The D band is due to defects in the crystalline structure. In MWCNT, the location of the D-band varies linearly depending on the laser excitation energy used in the test. Values between 1300 and 1360 have been reported[38;39]. In addition, CNT display another band at slightly less than double the wavelength of the D band. This band is called the G$'$ band and considered to be an overtone of the D band. The D band corresponds to one phonon scattering while the G$'$ band corresponds to two phonon scattering. While the D band represents the defects in a crystalline structure, the G$'$ band indicates long-range order in the system. Ramsn data for the materials tested is shown in Figure 4.3.

As expected, Raman Spectra of MWCNT, SWCNT and Graphite show G and D bands near 1580 and 1320 cm^{-1} as well as a G$'$ bear 2630 cm^{-1}. The height of the D band relative to the G band in MWCNT and SWCNT indicates more defective graphtic structure compared

to the graphite sample. CB does not show peaks in these locations because the carbon is not bonded together in a graphitic structure. As shown in Fig. 4.3b, the neat ABS sample also lacks the G and G′ band. However, the G band and D band are clearly present in the 15 wt% MWCNT composite, proving that the graphitic structure of the MWCNT is retained in the composite. However, the G′ peak disappears in this sample, because the concentration of MWCNT is not high enough to produce long range order.

4.3   TGA

Thermogravimetric Analysis(TGA) measures the decomposition of materials with increasing heat. This test provides data about the thermal stability of materials. It can also be used to calculate the composition of some materials. During TGA a small mass (1-50 mg) of the material is placed on a high precision scale is heated at a constant rate. As the temperature increases, the sample reacts with the atmosphere resulting in weight change. This data indicates over which temperature ranges the material is stable, and how cold it must b e kept to prevent reactions with the atmosphere. This lowest stable temperature is called the onset temperature T_{onset}, and can be estimated using the temperature at which the sample gains or loses 5% of its weight. The TGA data can also be used to calculate a samples composition. The purity of sample undergoing a known chemical reaction can be determine. When two components of a sample react independently at different temperatures, their contribution to the total mass can be analyzed, and the samples composition can be determined. TGA measures the thermal stability of materials. When two materials with significantly different decomposition temperatures are mixed, an estimate of the weight composition can be made. The two components will interact affecting the TGA curve. The materials may decompose in the same way that they do individually, or they may interact causing increased or reduced thermal stability. If the materials in a mixture decompose similarly to their independent behavior, and have significantly different T_{onset}s, and good estimate of the percentages of individual components can be made. The composite curve is treated as the superposition of the individual parts. When the composite material decomposes as a unit rather in stages

43

corresponding to each material, weight percentages cannot be accurately determined.

The TGA data shows the composite materials degrading in two stages. ABS/CNT composites have been documented to degrade in either one or two stages. Factors affecting whether this decomposition occurs in one or two stages include the ABS composition, i.e. ratios of acrylonitrile, butadiene, and styrene components, purging gas type, heating rate, and sample mass[40;41].

The TGA shown in Figure 4.4, indicates all composites containing 2.0 wt% or less of filler materials behave similarly to neat ABS. Differences between samples in this range are similar to variances between different samples of the same material. The samples with under2.0 wt% filler loading show an a T_{onset} around 380 °C following which they drop to an initial plateau of 7-9 mass % around 500 °C. Nearly all of this mass is burned off between 560 °C and 630 °C. So the majority of the polymer decomposes between 380 °C and 500 °C, and the remaining 7-9 % remains until 560 °C-630 °C.

As shown in Figure 4.4a Graphite loses than 5% of its mass in the temperature range studied. Meanwhile MWCNT and CB have onset temperatures near 505°C and 685 °C respectively. Addition of carbon fillers to ABS reduces the thermal stability, lowering T_{onset}. T_{onset} decreases with increasing filler concentration reaching 350°C for 5-15 wt% MWCNT and 360°C for 15-20% CB. Along with the shift T_{onset}, the 5-15 wt% MWCNT composite specimens show the second stable region or plateau shifted down to the 450-500°C range. A similar shift occurs in 7.5-10 wt% CB samples. These CB samples do not have a constant mass in the range, but do show a much slower rate of mass decrease in these regions. Samples with 5 wt% and up of filler material show increasing amounts of material remaining at this second plateau. These larger masses are attributed to the larger amounts of filler in the composite, which do not react at this temperature. This indicates the presence of more MWCNT or CB with increasing filler loading, but cannot be used to calculate the percentage of filler present in the material. At 800°C, a majority of the filler mass is present. However, the composite materials do not show significant increased mass retention at this temperature. So, ABS interacting with the material causes the carbon fillers to decompose at a lower temperature.
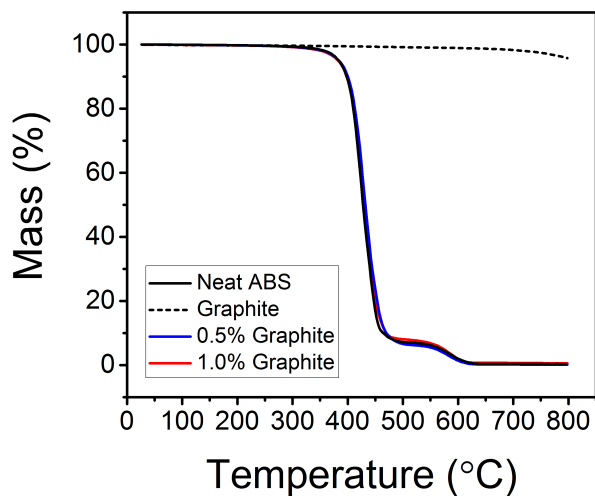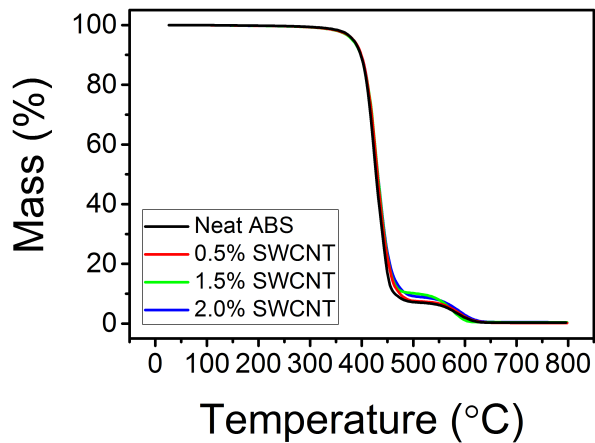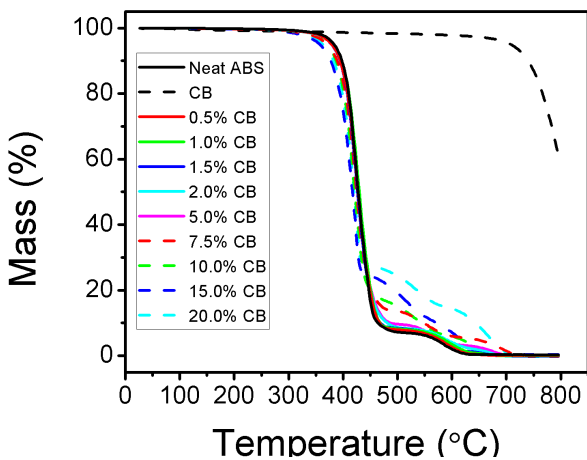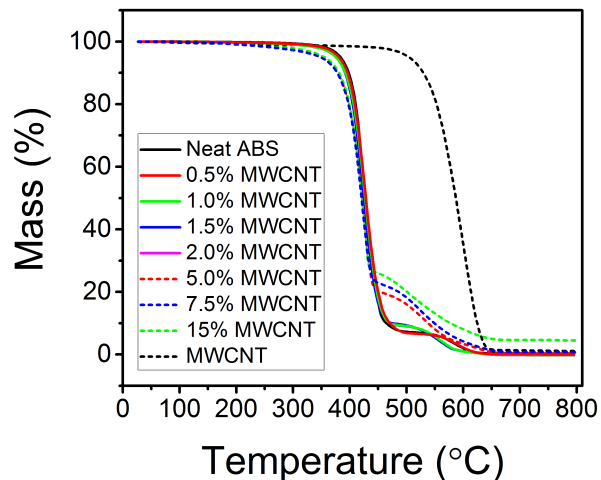
Figure 4.4: TGA data for a) graphite powder and Graphite/ABS composites b)SWCNT/ABS composites c) CB powder and CB/ABS composites and d) MWCNT powder and MWCNT/ABS composites

Table 4.1: Summary of TGA data

Material	T_{onset} (°C)	Mass % at Plateau		Difference between composite and neat at plateau (% mass)
		Mass % at 500 °C	Mass % at 460 °C	
Neat ABS	382.9	7.2	10.9	-
MWCNT powder	504	95.5	97.8	-
0.5 % MWCNT	381.1	6.9	-	-0.3
1.0% MWCNT	375.6	9.1	-	1.9
1.5% MWCNT	376.3	9.3	-	2.1
2.0% MWCNT	375.7	9.0	-	1.8
5.0% MWCNT	348.7	-	19.6	8.7
7.5% MWCNT	348.5	-	22.2	11.3
15.0% MWCNT	355.5	-	25.2	14.3
0.5% SWCNT	383.1	7.6	-	0.4
1.5% SWCNT	382.7	10.2	-	3
2.0% SWCNT	382.0	9.2	-	2
CB powder	686.0	98.3	-	-
0.5% CB	380.9	7.9	-	0.7
1.0% CB	381.3	8.2	-	1
1.5% CB	382.0	8.4	-	1.2
2.0% CB	379.2	8.6	-	1.4
5.0% CB	378.9	9.6	-	2.4
7.5% CB	378.5	13.6	-	6.4
10.0% CB	368.6	-	18.3	7.4
15.0% CB	357.3	-	23.7	12.8
20.0% CB	364.4	-	27.2	16.3
Graphite powder	>800	99.2	-	-
0.5% Graphite	384.2	6.6	-	-0.6
1.0% Graphite	382.9	8.1	-	0.9

Table 4.1 contains the onset temperature of sample at each wt%. It also shows the mass % of this sample in the stable region and compares the mass of composites in the stable region with the mass % of ABS at the same temperature. Based on the TGA data, the composite degrades at lower temperatures with the addition of carbon fillers. Since T_{onset} is over 100°C larger than the highest processing temperatures used in the material fabrication process, we conclude that minimal heat damage to the material occurs during this 3D printing process. The TGA data verifies that MWCNT and CB concentrations increase in the filament as more MWCNT and CB are added to the base. However, exact composition of the composite filament cannot be determined due to the interaction between the filler and ABS.

Chapter 5

Tensile Results

5.1 Tensile Tests

5.1.1 Expected Results

Mixing a high modulus reinforcing material with a high modulus, high strength material like carbon usually generates a material that is a hybrid of both properties. The interface transfers stress from the modulus to the reinforcement. As the filler concentration increases it contributes more of its properties to the composite. With increasing filler concentration, the ductility of the composite should decrease. The stiffness and strength of the material will increase as the filler concentration goes up and it carries more of the load. At filler concentrations exceeding a critical value, the strength will begin to decrease again

Recent results published by Oak Ridge National Laboratory showed an increase in strength of 5 MPa for 1.0 wt% CNT/ABS composites prepared using a twin-screw extruder. Increasing the concentration to 2.0 wt% caused a reduction in strength back to the original neat value[42].

5.1.2 Results

Overall the results show decreasing ductility with increasing filler concentration as predicted. However, the stiffness remains fairly constant while the strength generally decreases. Possible causes for this behavior are discussed in Section 5.1.4.

Neat ABS data

Eight AMSE D638 type IV tensile specimens were used to measure the baseline strength of FDM printed ABS. The ultimate tensile strength of the specimens clustered in two groups. The majority of the specimens had strengths of around 40.0 MPa, but there was a smaller cluster of samples with ulimate tensile strength at 43.9 MPa for an overall average of 40.1 MPa. The elastic modulus of the ABS ranged from 2.0 Gpa to 2.4 Gpa with an average value of 2.2 GPa. The breaking strain of the neat specimens ranged from 3.7-7.6% with an average of 5.1%.

CB tensile test data

Three ASME D638 type IV tensile test specimens with manufacture at CB filler concentrations of 0.5 wt% and 2.0 wt%. Two specimens were fabricated and tested at 5.0 wt% and 7.5 wt% CB and one at 10 wt%. These filaments were originally fabricated to test changes in conductivity with increasing filler concentration. For this reason, not enough material was available to produce three tensile test specimens. The test results are shown in Figure 5.1.

The average elastic modulus of the composite specimens initially declined to 2.1 and 2.0 Gpa for 0.5 wt% and 2.0wt%. Then it increased to a maximum value of 2.5 Gpa for 5.0 wt% and dipped to 2.3 GPa for both 7.5wt% and 10 wt% composite specimens. The ultimate strength showed similar behavior with strengths of 40.0 Mpa, 38.6 Mpa, 43.1 Mpa, 37.0 Mpa and 36.9 Mpa for 0.5 wt%, 2.0 wt%, 5.0 wt%, and 7.5 wt% CB specimens. The strain to failure generally declined with increasing filler concentrations. It started at 3.5 % for 0.5 wt% CB and declined to 2.5% for 10 wt%. The 2.0, 5.0, and 7.5 wt% specimens had average strain-to-falure points of 3.2%, 3.1% and 2.2% respectively.
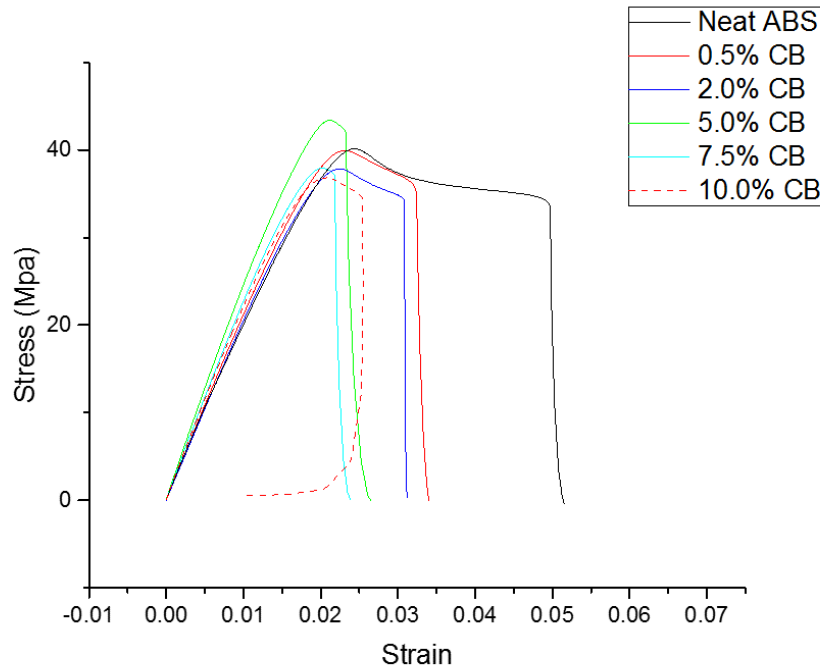
Figure 5.1: Graph comparing stress-strain curves of neat ABS and CB composite specimens

MWCNT tensile data

Three ASME D638 type IV tensile specimens were tested at MWCNT loadings of 0.5 wt%, 1.0 wt%, 1.5 wt%, 2.0 wt%, 5.0 wt%, and 7.5 wt%. Only one sample was fabricated at 15 wt% due to the small amount of material available. EIS data was the main focus for this 15 wt% composite material. The ultimate tensile strength of 0.5 wt% ranged from 32.3 MPa to 41.0 Mpa resulting in an average value of 35.5 MPa for an overall reduction in strength compared to the neat. The 1.0 wt% specimens improved to 35.7 MPa with a tighter range from 34.3 to 37.1 MPa. The 1.5 wt% specimens improved to an average of 36.5 MPa with a data range from 36.0 to 37.9 MPa. The average value reached a max at 2.0 wt% with a value of 37.4 wt% and a range of 35.7 to 38.5 Mpa. The 5 wt% specimen shows similar behavior with a range of 32.1 to 38.5 Mpa and average value of 35.9. Ultimate strength decreases slightly to 34.9 MPa for the 7.5 wt% samples to an average value. The 15 wt% specimen was extremely brittle with a ultimate strength of 17.6 Mpa. Two thirds of the specimens from 2.0 wt% to 7.5wt% have tensile strengths around 37-38 MPa, however the weakest specimen
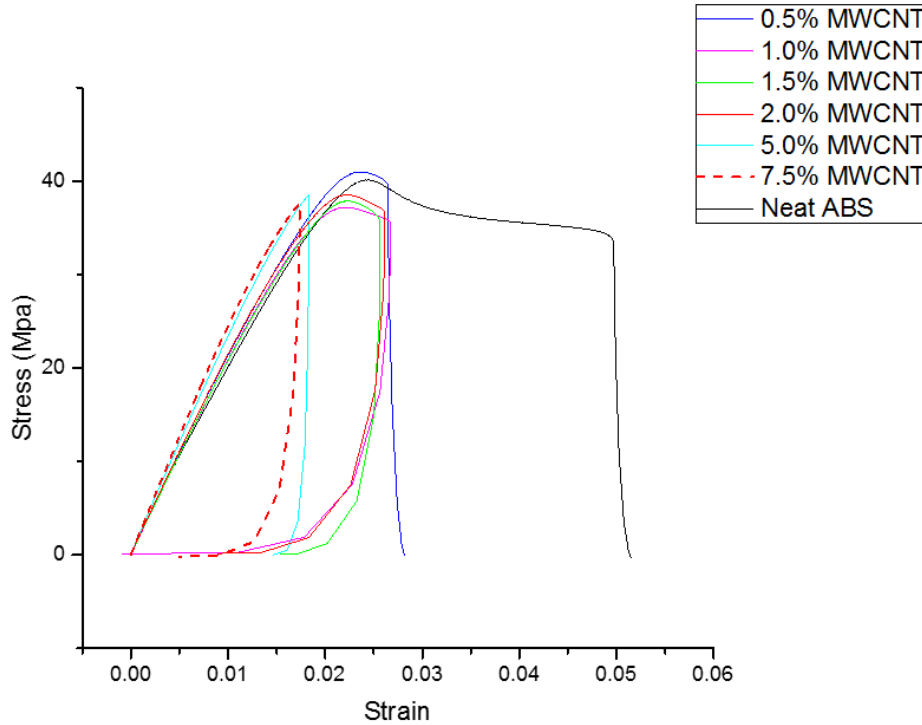
Figure 5.2: Graph comparing stress-strain curves of neat ABS and MWCNT composite specimens

in each group decreases strength dramatically with increasing filler concentration resulting in a significant reduction in average strength.

The elastic modulus of the MWCNT composite specimens initially dips with the addition of MWCNT filler, but gradually stiffens as the filler concentration increases. From the neat modulus of 2.2 GPa, the modulus drops to 2.0 GPa for 0.5 wt% and 1.0 wt%. The average elastic moduli for 1.5 wt% to 5.0 wt% MWCNT specimens similar to the neat ABS modulus with values of 2.1 GPa, 2.2 GPa, and 2.2 GPa for 1.5 wt%, 2.0 wt%, and 5 wt% respectively. The average value then increases to 2.3 GPa 7.5 wt% and 2.8 GPa for 15 wt% MWCNT composite specimens. These two weight percentages show both higher average and maximum elastic moduli compared to the neat specimens. So it is possible to increase the stiffness of FDM printed ABS plastic.

This improvement in elastic modulus comes with a substantial decrease in ductility as the strain to failure decreases with increasing filler concentration. Starting with at an average value of 5% for the neat specimens, the strain to failure decreases to 2.9% for 0.5 wt%

50

MWCNT and to 3.0% for 1.0 wt% MWCNT. THe downward trend continues with average strain to failures of 2.7%, 2.6%, 2.1%, 1.8%, and 0.66% for 1.5 wt%, 2.0 wt%, 5.0 wt%, 7.5 wt%, and 15.0 wt% MWCNT composite specimens respectively. From this data it is clear that the addition of even a small amount MWCNT filler significantly reduces the ductility of the polymer matrix. This effect is more pronounced with the inclusion of more filler material.

As shown in Fig. 5.2 the neat ABS samples display ductile behavior. This gradually transitions to more brittle behavior until by 7.5 wt% typical brittle behavior is observed.

5.1.3 Oven and microwave data

An additional two tensile specimens were fabricated at MWCNT loadings of 0.5 wt%, 1.0 wt%, 1.5 wt%, 2.0 wt%, 5.0 wt%, and 7.5 wt%. Before testing, these specimens were microwaved for 3 seconds. The motivation for this treatment was CNT's high microwave absorptivity. The goal was to cause localized melting in the part to bond the rasters together and create better interlayer bonding. The results of these tests are shown in Figure 5.3a and5.3b

The initial tensile tests of the microwaved specimens showed no improvement from the unheated specimens. So, an additional heat treatment was applied to the 1.5 wt% and 2.0 wt% specimens as an effort to improve strength and ductility. These specimens were placed in a oven at 135 $^{\circ}C$ for 1 hr. This treatment caused the specimen to become soft but was sufficiently below the T_g to avoid melting. Minimal warping at the edge of the specimens was observed, but the gage section was not affected. The goal of this heat treatment was to cause the rasters to fuse together. Neat ABS specimens were subjected to both heat treatments to isolate the role of CNT in the heating process.

ASME D638 type V specimens

After testing the Type IV results, several type V specimens were tested. The smaller size of these test samples affords less opportunity for large defects. So, these specimens might show better properties than their larger counterparts. Three neat ABS specimens were tested

(a)

(b)

(c)
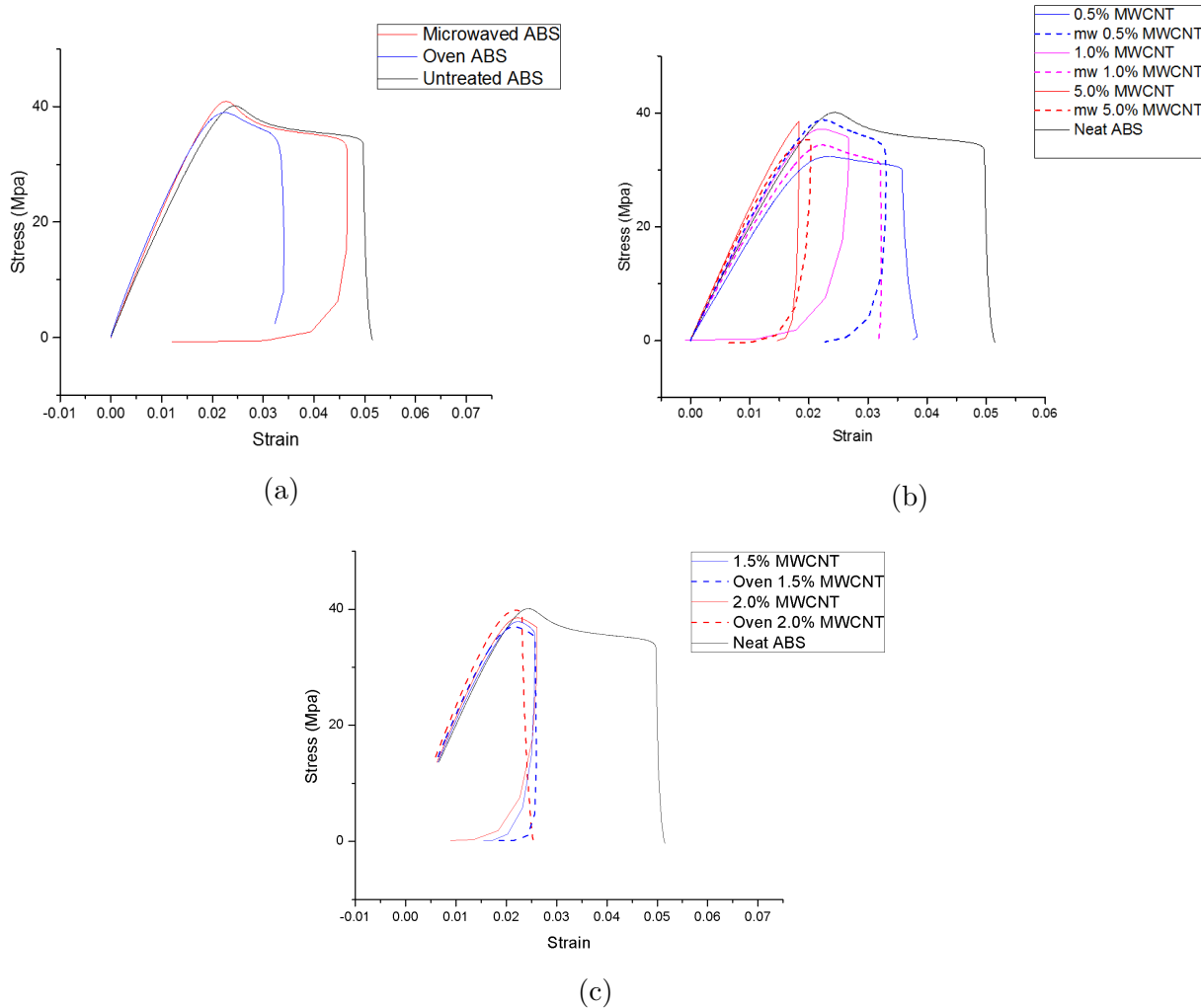
Figure 5.3: Stress-strain curves comparing (a) untreated neat ABS specimens with oven and microwaved specimens (b) microwaved and non-microwaved composite specimens (c) untreated and oven-treated composite specimens.
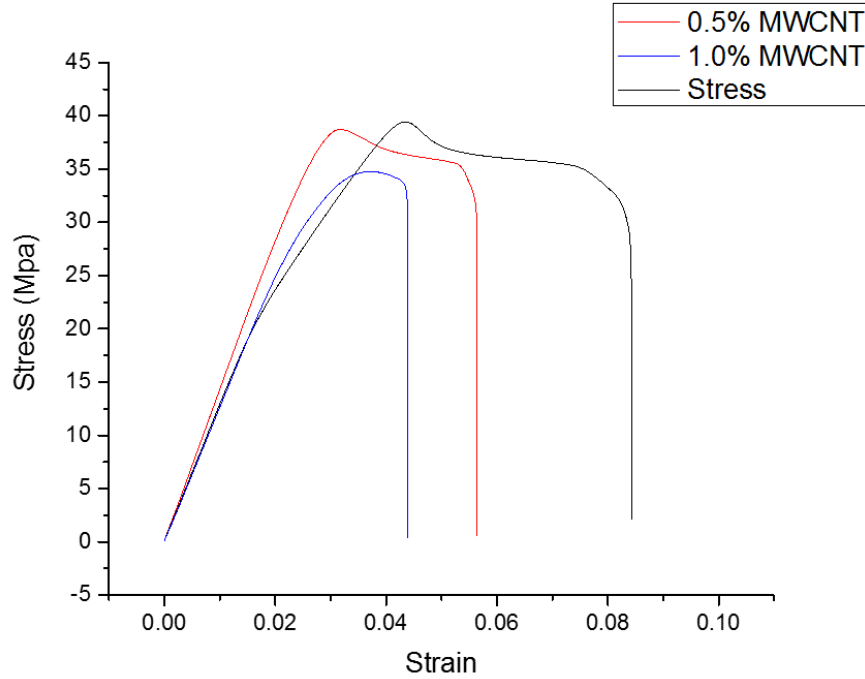
Figure 5.4: Graph comparing stress-strain curves of neat ABS and MWCNT D638 Type V composite specimens

to form a baseline. Then, three 0.5 wt% MWCNT and three 1.0 wt% MWCNT type V samples were compared resulting in the graph in Figure 5.4. For neat ABS, the average elastic modulus was 1.3 Gpa, the average ultimate strength was 38.1 MPa, and the average strain to failure was 7.8%. The 0.5 wt% MWCNT elastic modulus varied from 1.1 Gpa to 1.4 Gpa with an average value of 1.2 Gpa, and the ultimate strength varied from 25.6 Mpa to 38.7 Mpa. Meanwhile the strain to failure ranged from 3.2 %to 5.9% with an average of 4.9%. One of the specimens significantly underperformed the rest of the specimens in all of these areas, possibly due to poor printing. As shown in Figure 5.4, the 0.5wt% MWCNT specimen shows much less strain hardening than the ABS specimen. A similar ultimate strength was achieved around 2 % strain lower than for the neat ABS. So, this composite will deform less under load than neat ABS. The 1.0 wt% MWCNT had a elastic modulus of 1.2 Gpa, an ultimate tensile strength of 34.6 MPa, and a strain to failure of 4.4 %.

So for the smaller type V test specimens, the elastic modulus gradually decreased with increasing filler concentration while the strain to failure declines. Although the 0.5 wt%
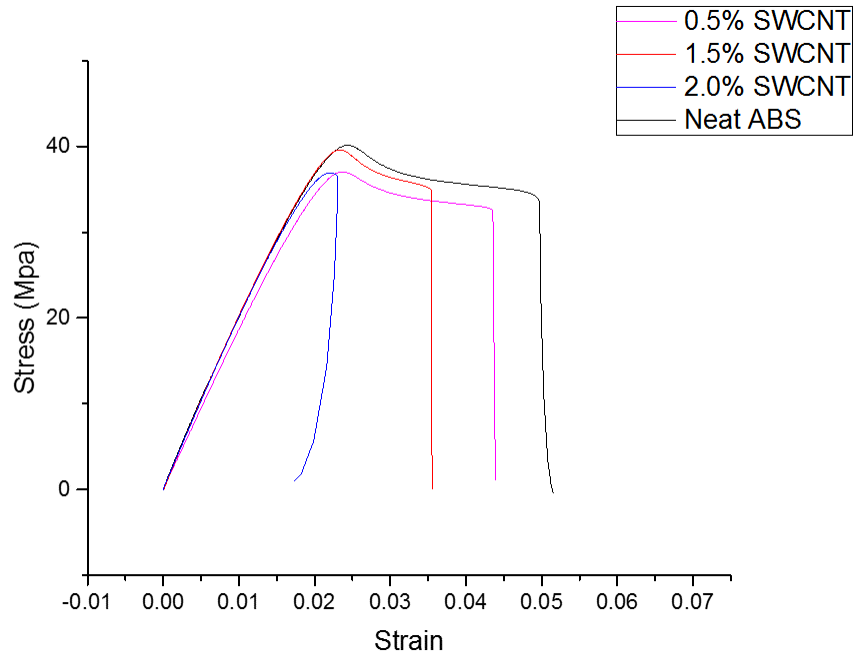
Figure 5.5: Graph comparing stress-strain curves of neat ABS and SWCNT composite D638 type IV specimens

MWCNT had a similar range of tensile strength to the neat ABS, the stregth declined for the 1.0wt% composite. The most significant result was the reduced strain to ultimate strength observed in the 0.5 wt% MWCNT composite.

SWCNT tensile data

Three 2.0wt% and two 1.5 wt% and 1.0 wt% tensile test specimens were tested. The resulting data is shown in Fig. 5.5. The SWCNT composite specimens showed a trend in decreasing ductility. The 0.5 wt% SWCNT composite had 27% reduction in breaking strain compared to neat ABS. This increased to 46% and 49% reduction for 1.5 wt% and 2.0 wt% respectively. The ultimate strength was 39.5 MPa for 0.5 wt% SWCNT and reduced to 36.3 Mpa for 2.0 wt% SWCNT. The 1.5 wt% SWCNT composite specimens had similar ultimate strength to the neat ABS specimens at 39.5 MPa. The 1.5 wt% and 2.0wt% composites showed similar elastic moduli to neat ABS while the 0.5% SWCNT composite material's modulus decreased.

5.1.4 Discussion

For filler properties to be transferred to the composite, good interfacial adhesion and dispersion are required. If the interfacial adhesion between the phases is low, the filler material induces stress concentrations by acting as holes or nanostructured flaws[22]. This can be improved by increasing the surface area of the particle to transmit more shear forces or by improving the bonding between filler materials and the polymer matrix[22;43]. Interfacial adhesion arises through the following mechanisms:

- Electrostatic and van der Walls interactions between the filler and the matrix. These occur in the absence of chemical bonding and are the primary load transfer mechanism for CNT/polymer composites[22;43;44].

- Micromechanical interlocking due to surface roughness at the interface. Since CNT are smooth, these are minimal for CNT/polymer composites[22].

- Chemical bonding between filler materials and matrix. This is the strongest, but is not guaranteed to be present.[22]

Agglomerated carbon nanofillers are held together by weak Van der Waals forces. When agglomerates are present, separation of the agglomerated bundle can be the failure mechanism rather than failure of the filler material. When this happens, the composites strength is greatly reduced[22;44]. For MWCNT, concentric shells may slip against each other resulting in a telescope-like elongation. This also has the potential to reduce mechanical properties. Agglomeration effects can be reduced by improving the dispersion of nanoparticles in the matrix. Cross-linking MWCNT shells or nanofiller bundles together reduces the amount of slipping occurring in the filler material. However, crosslinking of graphitic materials introduces defects into the crystalline structure, which will negatively impact the mechanical properties of the individual molecules[22].
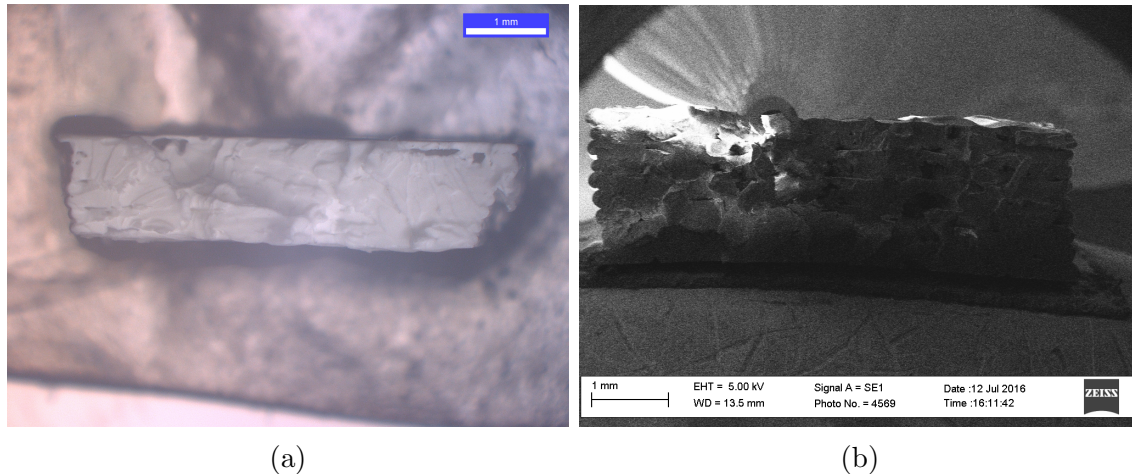
Figure 5.6: Fracture surface images of neat ABS specimens (a)Optical microscope image (b) SEM image

5.2 Fracture Surface Images

Fracture surface images can provide information about the cause and type of failure in a material. It can be used to identify voids or crack initiation points. In composites, pictures of broken fibers in the matrix provide information about the interface strength. If they pull out from the matrix rather than breaking flush with it, this indicates that the interface is not strong enough to transfer the load to the fibers.

Pictures of neat specimen in Figure 5.6 reveal that the rasters were well fused together by the FDM printing process. The sides have more defined rasters than the interior of the part, probably due to faster cooling during the printing process. Voids are evident in the fracture surface images.

Figure 5.7 compares the fracture surface a of 0.5% graphite specimen with those of the 2.0 wt% CB, MWCNT, and SWCNT specimens. The graphite specimen in Figure 5.7a shows a large chunk of graphite in the lower left corner. All of the composite specimens show contain specks of dark material not observed in the neat specimens. Presumably these are due high concentrations of ller material in these areas. These inhomogeneous areas suggest that the filler material is agglomerating in those locations, thereby weakening the material. However the MWCNT and SWCNT specimens display large dark areas which span several rasters. This suggests that they were formed after extrusion from the printer nozzle, rather
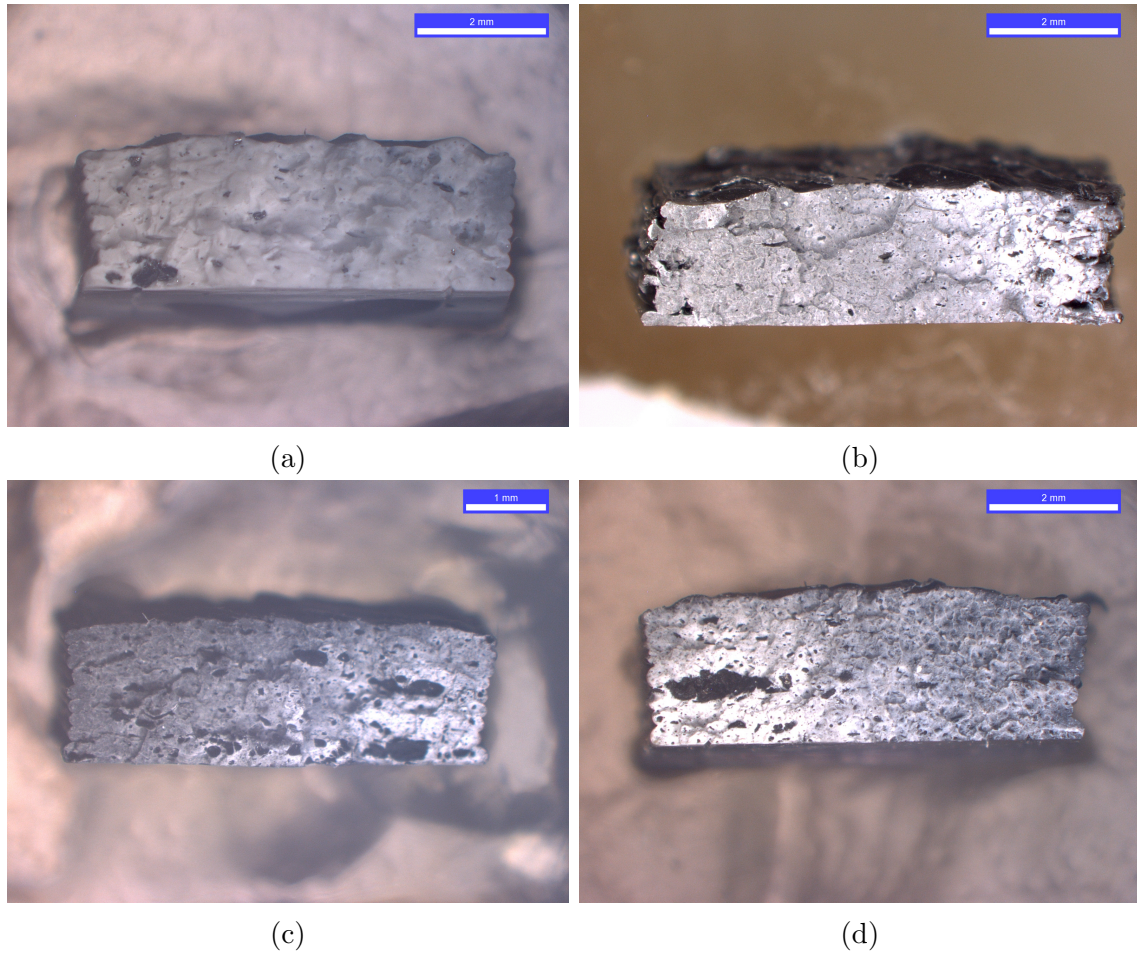
Figure 5.7: Optical Microscope images of (a)0.5 % Graphite (b) 2.0% CB (c) 2.0%MWCNT and (d) 2.0% SWCNT

than being defects contained in the filament. More study is required to determine if they are in fact agglomerations of nanomaterials or optically dark by another mechanism. The composite ABS material is black after printing, but turns white at areas of high stress. So, it could also be possible that the optically dark spots visible in the microscope represent unequal stress throughout the cross-section. If the printing process is depositing large agglomerations across multiple rasters, identifying and eliminating the process by which this occurs would be imperative for further material development.

While the composite specimens in Figure 5.7 specimens lack the larger voids noticed in the neat specimens, they do contain small voids at the intersections of the rasters. The MWCNT and CB specimen show a flatter surface than neat and 0.5% MWCNT specimens suggesting

57

a more brittle fracture. The SWCNT specimen in Figure 5.7d shows a unique region of high roughness on the right side which could indicate ductile behavior on the microscale or rapid fracture in this area. This surface is significantly different from the fracture surfaces observed in all other specimens.

Figure 5.8 shows fracture surface images of higher weight percentage specimens. Figure 5.8c and 5.8f are good examples of the small voids between adjacent rasters present to some extent in all the composite samples. In these two samples, lines marking the separation can be observed in the cross-section. This indicates that the layers were not well bonded in these two samples. Metallic reflections and discolorations in the optical microscope images can be attributed to the presence of carbon fillers. The flat fracture surface is consistent with the brittle failure observed in the tensile tests.

Figure5.9 shows the fracture surface of the some heat treated specimens. These fracture surfaces are similar to the untreated specimens. The oven ABS specimen shows some voids attributed to under-extrusion in the manufacturing process towards the top of the image. The oven 2.0 % MWCNT shows fewer and smaller dark spots than the untreated specimen.

5.3   Electrical Impedance Spectroscopy

Graphite and MWCNT specimens were tested at all weight percentages. Specimens under 5 wt% showed test results very similar to neat ABS. The real part,σ, of the complex electrical conductivity of these materials is frequency dependent. Below a critical frequency, ω_c, the conductivity is constant. This frequency independent value is the DC conductivity, $\sigma_d c$. The definition of the critical frequency was proposed by Kilbride et al.[45] to be $\sigma(\omega_c) = 1.1\sigma_d c$. Above ω_c, the conductivity increases exponentially with increasing frequency.

e

In Figure 5.10, the 7.5 wt% MWCNT shows this typical material behavior. For other sepcimens, the frequency range tested shows only a segments of the frequency responce. Lower weight percentages show only the exponentially increasing conductivity and 15 wt% MWCNT composite data shows mainly the constant conductivity region. The AC conduc-
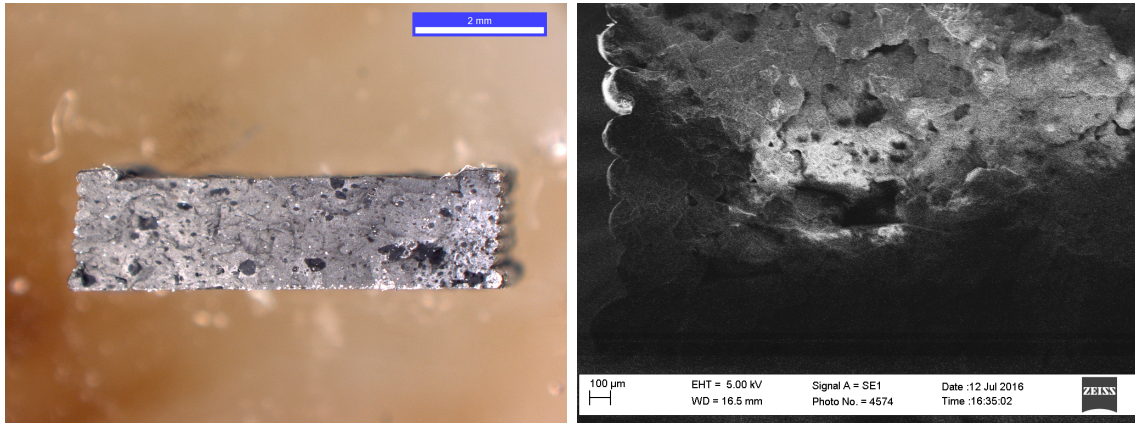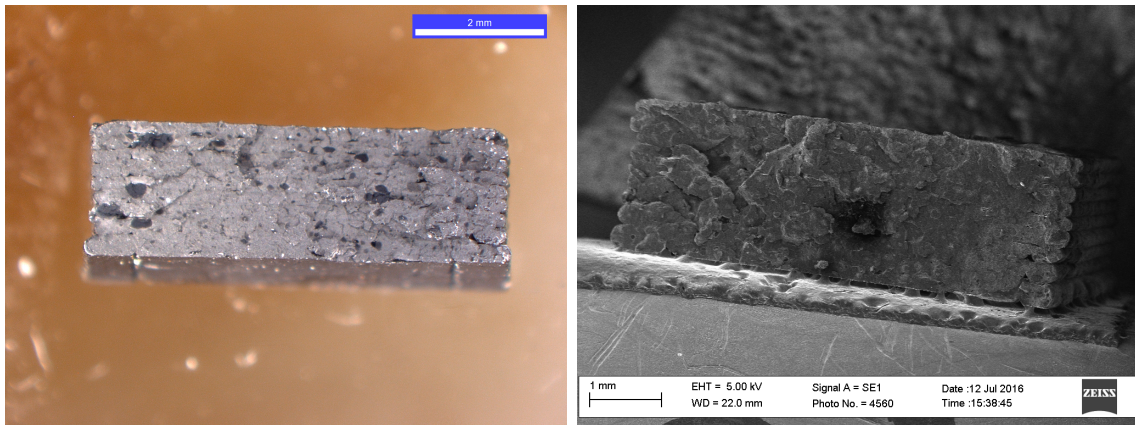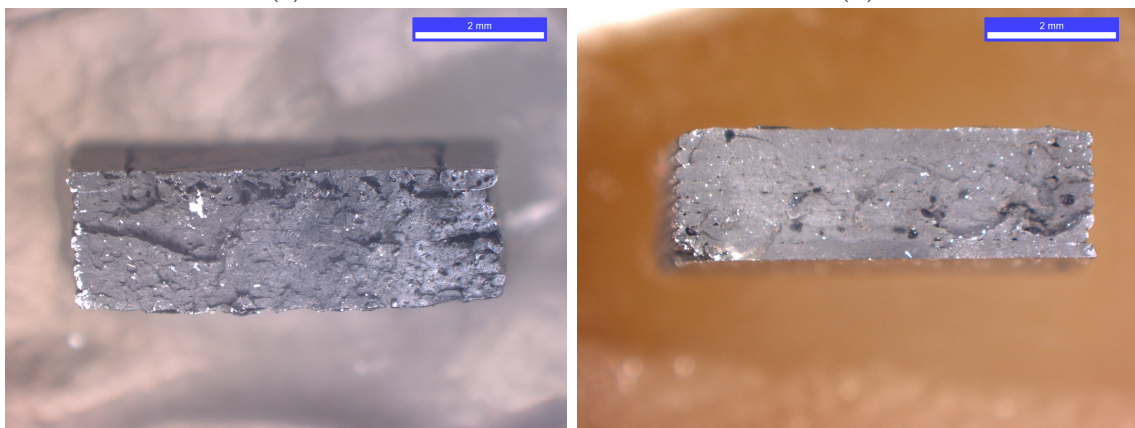
Figure 5.8: Fracture surface images of high weight percentage specimens (a)Optical microscope and (b)SEM images of 5.0% MWCNT (c)Optical microscope and (d)SEM images of 7.5% MWCNT (e) Optical microscope image of 10.0%CB (f) Optical microscope image of 15.0%MWCNT
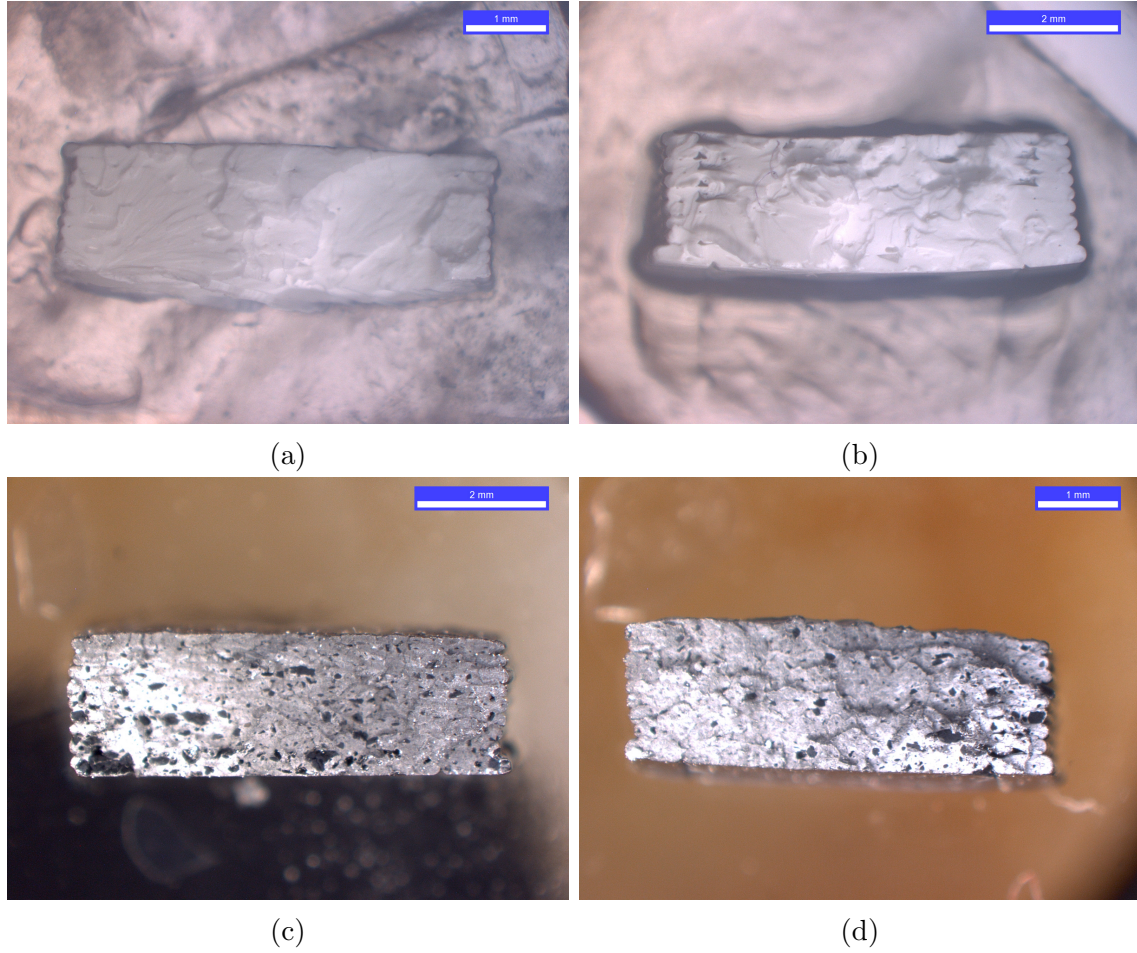
Figure 5.9: Optical microscope images of (a) microwaved ABS specimen (b) oven ABS specimen (c) microwaved 5.0%MWCNT/ABS composite specimen and (d) oven 2.0% MWCNT/ABS composite specimen

tivity's dependence on frequency can be modeled with the equation

$$\sigma(\omega) = \omega_d c + A\omega^s \tag{5.1}$$

where A and s are constants. Curve fitting of the collected data gives the values of A, s and $\sigma_d c$ shown in Table 5.1. Note that the conductivity of polymers is affected by temperature as well as frequency. A slight increase in the conductivity of the 15 wt% sample at high frequencies indicates that the critical frequency is $1.1x10^6$ rad/s or 180 kHz. With such a high critical frequency the exponential portion of the curve more difficult to observe than the other specimens. The 0.5 wt% Graphite, 1.0 wt% Graphite, and 0.5-2 wt% MWCNT
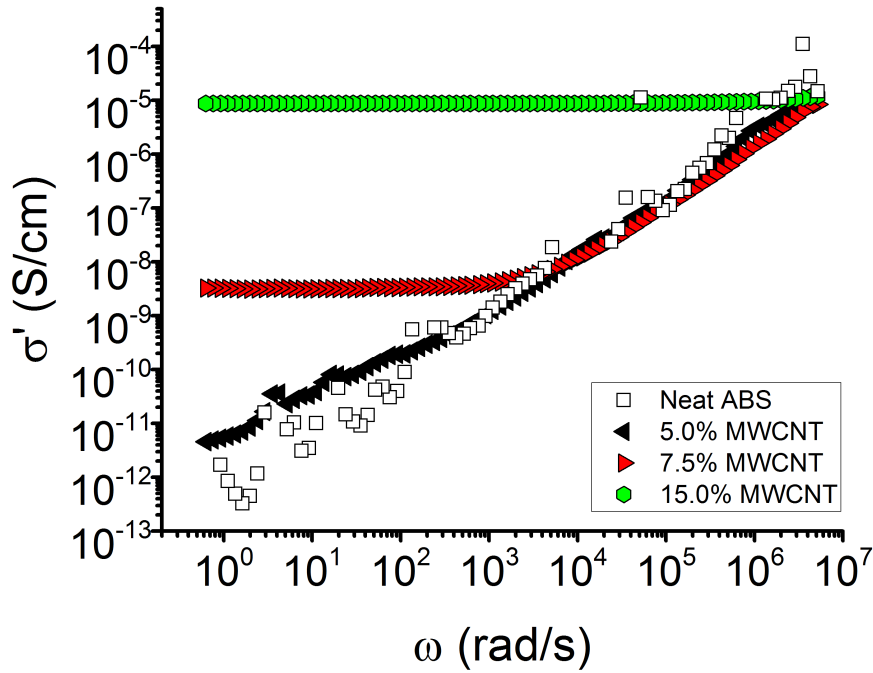
Figure 5.10: AC conductivity data for MWCNT composites.

specimens all showed similar behavior to the neat ABS sample shown in Figure 5.10. For all materials tested under 5.0 wt%, the frequency independent stage occurs at lower frequencies than studied. In the frequency independent range, the material acts as a resistor while at higher frequencies it acts like a capacitor. The results of the impedance testing show that $\sigma_d c$ and ω_c increase with increasing wt% of MWCNT. This increase of conductivity is expected due to the presence of nanotubes in the filler.

Conduction in the frequency independent region is due to direct contact between MWCNT. Higher values correspond to a more extensive network of MWCNT[46]. Conduction due to tunneling electrons between particles increases with increasing frequency and accounts for part of the frequency dependent component of the conductivity. Reduced charge buildup from space charges occurrs with increasing frequency and also contributes to the increasing conductivity[47]. Based on the data aquired, the MWCNT forms a better network at higher weight percentages, causing an increase in the DC conductivity. Composites tested below 5 wt% showed very little difference from neat ABS in the regions studied. 7.5 wt% and 15

61

Table 5.1: Summary of EIS data

Material	σ_{dc} (S/cm)	ω_c (rad/s)	s	A (S/cm)
Neat ABS	---	---	1.1	8×10^{-13}
5.0 wt% MWCNT	--	--	1.0	2×10^{-12}
7.5 wt% MWCNT	3.2×10^{-9}	437	1.13	2×10^{-13}
15 wt% MWCNT	8.7×10^{-6}	1.1×10^6	0.81	1×10^{-11}

wt% MWCNT specimens show increased conductivity. 15 wt% has DC conductivity in the semi-conducting range.

Chapter 6

Conclusions and Recommendations

The purpose of this research was to determine the effect of carbon fillers on mechanical and electrical properties of FDM printed ABS composite materials. SEM was used to characterize the nanomaterials, and XRD, TGA, and Raman were used to confirm the presence of filler material in the composite materials. Tensile testing showed improvement in tensile strength for 5.0 wt% Carbon Black Specimen and 0.5 % MWCNT Type V specimen. Fracture surface images showed good adherence between layers and rasters. Small voids were present at the interface of rasters. Microwave and oven heat treatments were applied in an effort to promote fusion of rasters and improve the mechanical properties of the material. Fracture surface images showed little improvement, but stiffness increased due to oven treatment. EIS data shows strong improvement in electrical conductivity of MWCNT/ABS composite material with increasing weight percentage. The 15 wt% MWCNT had a DC conductivity of $8.74x10^-6$ S/cmcompared to the neat ABS conductivity of $< 10^-12$ S/cm. Graphite and MWCNT composites containing 2.0 wt% or less of filler material had similar electrical properties to neat ABS Recommendation for further research on carbon filler FDM printed composites include:

- Take high magnification images of the composite material. These images could help determine the level of dispersion or agglomeration of filler materials in the sample. Gaining more insight into the materials structure would help engineer solutions.

- Work to improve filler material dispersion. Use higher shear mixing process or functionalize nanomaterials to facilitate dispersion in the matrix.

- Vary matrix material to find optimal. Make specimens at a low weight percentage of the same nanomaterial in each of the common FDM stock materials to determine which bonds best with the material.

- Vary the aspect ratio of the nanomaterials used. If the material is below its critical length, increasing the aspect ratio will improve load transfer from the matrix to the filler. Also, higher aspect ratios are more expensive and more likely to break during processing, so determining the most effective length would result in cost savings.

Bibliography

[1] Carnegie Mellon University David Touretzky, School of Computer Science. Stl files and slicing software, 2016. URL https://www.cs.cmu.edu/afs/cs/academic/class/15294t-s16/lectures/stl/stl.pdf. Online; accessed 28-July-2016.

[2] Paul Trani. Getting started with 3d printing. *How Design*, August 4 2015. URL http://www.howdesign.com/web-design-resources-technology/how-to-3d-print-what-is-3d-printing/. Online; accessed 27-July-2016.

[3] University of Cambridge: Phase Transformations Complex Properties Research Group. Bearing fabrication by three-dimensional printing. URL http://www.msm.cam.ac.uk/phase-trans/2015/bogey/index.html. Online; accessed 27-July-2016.

[4] Science in Public. The world's first printed jet engine, February 16 2015. URL http://www.scienceinpublic.com.au/media-releases/monash-avalonairshow-2015. Online; accessed 27-July-2016.

[5] Klaus Cicha, Zhiquan Li, Klaus Stadlmann, Aleksandr Ovsianikov, Ruth Markut-Kohl, Robert Liska, and Júrgen Stampfl. Evaluation of 3d structures fabricated with two-photon-photopolymerization by using ftir spectroscopy, September 2011.

[6] Kaufui V. Wong and Aldo Hernandez. A review of additive manufacturing. *International Scholarly Research Network Mechanical Engineering*, pages 1–10, 2012.

[7] L. Novakova-Marcincinova, J. Novak Marcincin, J. Barna, and J. Torok. Special materials used in fdm rapid prototyping technology application. In *IEEE 16th International Conference on Intelligent Engineering Systems*, INES '12.

[8] Tess. Type a machines redefines 3d printing infill with absolute dimensions and 3d internal structures. *3ders.org*, May 18 .

[9] Hua Liu and L. Catherine Brinson. Reinforcing efficiency of nanoparticles: A simple comparison for polymer nanocomposites. *Composites Science and Technology*, 68:1502–1512, 2008.

[10] University of Cambridge: Department of Engineering. Specific stiffness - specific strength, 2002. URL http://www-materials.eng.cam.ac.uk/mpsite/interactive_charts/spec-spec/basic.html. Online; accessed 27-July-2016.

[11] Columbia University. Laser machining process. URL http://www.aml.engineering.columbia.edu/ntm/level1/ch05/html/l1c05s03.html. Online; accessed 28-July-2016.

[12] B'ela Suki. The major transitions of life from a network perspective. *Frontiers in Physiology*, 3:1–13, 2012.

[13] Jie Chen, Xue-Chong Du, Wen-Bin Zhang, Jing-Hui Yang, Nan Zhang, Ting Huang, and Yong Wang. Synergistic effect of carbon nanotubes and carbon black on electrical conductrivity of pa6/abs blend. *Composites Science and Technology*, 81:1–8, 2013.

[14] Huan Pang, Ling Xu, Ding-Xiang Yan, and Zhong-Ming Li. Conductive polymer composites with segregated structures. *Progress in Polymer Science*, 39(11).

[15] P A Martins-J'unior, C E Alacâtara, R R Resende, and A J Ferreira. Carbon nanotubes: Directions and perspectives in oral regenerative medicine. *Journal of Dental Research*, 20:1–9, 2013.

[16] Rajarshi Chakrabarti, Jean-Yves Delannoy, Marc Couty, and Kenneth S. Schweizer. Packing correlations, collective scattering and compressibility of fractal-like aggregates in polymer nanocomposites and suspensions. *Soft Matter*, 7:5397–5407, 2011.

[17] Lamuel Abraham David. Synthesis of large-area few layer graphene films by rapid heating and cooling in a modified apcvd furnace. Master's thesis, Kansas State University, Manhattan, Kansas, USA, 2011.

[18] Basheer Alshammari. *Processing, Structure and Properties of Poly (ethyleneterephtha-late)/Carbon Micro-and Nano-composites*. PhD thesis, The University of Manchester, 2015.

[19] Matthias Gurr, Daniel Hofmann, Michael Ehm, Yi Thomann, Rainer Kübler, and Rolf Mülhaupt. Acrylic nanocomposite resins for use in stereolithography and structural light modulation based rapid prototyping and rapid manufacturing technologies. *Advanced Functional Materials*, 18:2390–2397, 2008.

[20] Ángel Ramón Torrado Pérez. *Defeating Anisotropy in Material Extrusion 3D Printing via Materials Development*. PhD thesis, The University of Texas at El Paso, Ann Arbor, Michigan, USA, 5 2015.

[21] Bodo Fiedler, Florian H. Gojny, Malte H. G. Wichmann, Mathias C. M. Nolte, and Karl Schulte. Fundamental aspects of nano-reinforced composites. *Composites Science and Technology*, 66:3115–3125, 2006.

[22] O. Breuer and Uttandaraman Sundararaj. Big returns from small fibers: A review of polymer/carbon nanotube composites. *Polymer Composites*, 25(6):630–645, 2004.

[23] Syed KH Gulrez, ME Ali Mohsin, Hamid Shaikh, Arfat Anis, Anesh Manjaly Pulose, Mukesh K Yadav, Eng Hau P Qua, and SM Al-Zahrani. A review on electrically conductive polypropylene and polyethylene. *Polymer Composites*, 35(5):900–914, 2014.

[24] Chong Gao, Shimin Zhang, Feng Wang, Bin Wen, Chunchun Han, Yanfen Ding, and Mingshu Yang. Graphene networks with low percolation threshold in abs nanocomposites: Selective localization and electrical and rheological properties. *American Chemical Society: Applied Materials Interfaces*, 6:12252–12260, 2014.

[25] Somayeh Taheri, Ehsan Nakhlband, and Hossein Nazockdast. Microstructure and multiwall carbon nanotube partitioning in polycarbonate/acrylonitrile-butadiene-styrene/multiwall carbon nanotube nanocomposites. *Polymer-Plastics Technology and Engineering*, 52:300–309, 2013.

[26] Romil Bhandavat. *Molecular Precursor Derived SIBCN/CNT and SIOC/CNT Composite Nanowires for Energy Based Applications*. PhD thesis, Kansas State University, Manhattan, Kansas, USA, 2013.

[27] Asima Naz, Ayesha Kausar, Muhammad Siddiq, and Muhammad Aziz Choudhary. Comparative review on structure, properties, fabrication techniques, and relevance of polymer nanocomposites reinforced with carbon nanotube and graphite fillers. *Polymer-Plastics Technology and Engineering*, 55(2).

[28] Angel R. Torrado Perez, David A. Roberson, and Ryan B. Wicker. Fracture surface analysis of 3d-printed tensile specimens of novel abs-based materials. *Journal of Failure Analysis and Prevention*, 14:343–353, 2014.

[29] Halil L. Tekinalp, Vlastimil Kunc, Gregorio M. Velez-Garcia, Chad E. Duty, Lonnie J. Love, Amit K. Naskar, Craig A. Blue, and Soydan Ozcan. Highly oriented carbon fiber–polymer composites via additive manufacturing. *Composites Science and Technology*, 105:144–150, 2014.

[30] M. L. Shofner, K. Lozano, F. J. Rodríguez-Macías, and E. V. Barrera. Nanofiber-reinforced polymers prepared by fused deposition modeling. *Journal of Applied Polymer Science*, 89:3081–3090, 2003.

[31] M. L. Shofner, F. J. Rodríguez-Macías, R. Vaidyanathan, and E. V. Barrera. Single wall nanotube and vapor grown carbon fiber reinforced polymers processed by extrusion freeform fabrication. *Composites Part A: applied science and manufacturing*, 34:1207–1217, 2003.

[32] Runqing Ou, Rosario A Gerardt, Courtney Marrett, Alexandre Moulart, and Jonathan S Colton. Assessment of percolation and homogeneity in abs/carbon black composites by electrical measurements. *Composites Part B: Engineering*, 34:607–614, 2003.

[33] George Tsiakatouras, Eirini Tsellou, and Constantinos Stergiou. Comparative study

on nanotubes reinforced with carbon filaments for the 3d printing of mechanical parts. *World transactions on Engineering and Technology Education*, 12(3):392–396, 2014.

[34] Xiaojun Wei, Dong Li, Wei Jiang, Zheming Gu, Xiaojuan Wang, Zengxing Zhang, and Zhengzong Sun. 3d printable graphene composite. *Scientific Reports*, 105(11181):1–7, 2015.

[35] Z.Q. Li, C. J. Lu, Z. P. Xia, Y. Zhou, and Z. Luo. X-ray diffraction patterns of graphite and trubostratic carbon. *Carbon*, 45:1686–1695, 2007.

[36] T. Belin and F. Epron. Characterization methods of carbon nantubes: a review. *Materials Science and Engineering B*, 119:105–118, 2005.

[37] Dilip K. Singh, P. K. Iyer, and P. K. Giri. Diameter dependence of interwall separation and strain in multiwalled carbon nanotubes probed by x-ray diffraction and raman scattering studies. *Diamond Related Materials*, 19:1281–1288, 2010.

[38] L Bokobza and J Zhang. Raman spectroscopic characterization of multiwall carbon nanotubes and of composites. *Express Polym. Lett*, 6(7):601–608, 2012.

[39] R Saito, A Grüneis, Ge G Samsonidze, VW Brar, G Dresselhaus, MS Dresselhaus, A Jorio, LG Cançado, C Fantini, MA Pimenta, et al. Double resonance raman spectroscopy of single-wall carbon nanotubes. *New Journal of Physics*, 5(1):157, 2003.

[40] Mohammed H. Al-Salah, Bader A. Al-Saidi, and Raed M. Al-Zoubi. Experimental and theoretical analysis of the mechanical and thermal properties of carbon nanotube/acrylonitrile–styrene–butadiene nanocomposites. *Polymer*, 89:12–17, 2016.

[41] Brajesh K. Singh, Prativa Kar, Nilest K. Shrivastava, Susanta Banerjee, and Bhanu B. Khatua. Electrical and mechanical properties of acrylonitrile-butadiene-styrene/multiwall carbon nanotube nanocomposites prepared by melt-blending. *Journal of Applied Polymer Science*, 124:3165–3174, 2012.

[42] Paul A. Menchhofer, Joseph E. Johnson, and John Lindahl. Carbon nanotube chopped fiber for enhanced properties in additive manufacturing. Master's thesis, Oak Ridge National Laboratory, Oak Ridge,Tennessee, USA, 2016.

[43] J-H. Du, J. Bai, and H-M. Cheng. The present status and key problems of carbon nanotube based polymer composites. *eXPRESS Polymer Letters*, 1(5).

[44] Mohammad Moniruzzaman and Karen I. Winey. Polymer nanocomposites containing carbon nanotubes. *Macromolecules*, 39:5194–5205, 2006.

[45] B. E. Kildbride, J. N. Coleman, J. Fraysse, P. Fournet, M. Cadek, A. Drury, S. Hutzler, S. Roth, and W.J. Blau. Experimental observation of scaling laws for alternating current and direct durrent conductivity in polymer-carbon nanotube composite thin films. *Journal of Applied Physics*, 92(7).

[46] Mohammed H. Al-Salah, Haya K. Al-Anid, Yazan A. Husain, Hasan M. El-Ghanem, and Saadi Abdul Jawad. Impedance characteristics and conductivity of cnt/abs nanocomposites. *Journal of Physics D: Applied Physics*, 46(385305):1–8, 2013.

[47] Mohammed H. Al-Salah and Saadi Abdul Jawad. Graphene nanoplatelet–polystyrene nanocomposite: Dielectric and charge storage behaviors. *Journal of Electronic Materials*, 45:3532–3539, 2016.